UNRAVELING EXCITONIC DYNAMICS OF SOLUTION-PROCESSED QUANTUM WELL STACKS

A THESIS SUBMITTED TO

THE GRADUATE SCHOOL OF ENGINEERING AND SCIENCE

OF BILKENT UNIVERSITY

IN PARTIAL FULFILLMENT OF THE REQUIREMENTS FOR

THE DEGREE OF

MASTER OF SCIENCE

IN

ELECTRICAL AND ELECTRONICS ENGINEERING

By

Onur Erdem

July, 2015

UNRAVELING EXCITONIC DYNAMICS OF SOLUTION-PROCESSED QUANTUM WELL STACKS

By Onur Erdem

July, 2015

We certify that we have read this thesis and that in our opinion it is fully adequate, in scope and in quality, as a thesis for the degree of Master of Science.

Assoc. Prof. Dr. Hilmi Volkan Demir(Advisor)

Assoc. Prof. Dr. Dönüş Tuncel

Assist. Prof. Dr. Nihan Kosku Perkgöz

Approved for the Graduate School of Engineering and Science:

Prof. Dr. Levent Onural
Director of the Graduate School

ABSTRACT

UNRAVELING EXCITONIC DYNAMICS OF SOLUTION-PROCESSED QUANTUM WELL STACKS

Onur Erdem
M.S. in Electrical and Electronics Engineering
Advisor: Assoc. Prof. Dr. Hilmi Volkan Demir
July, 2015

Colloidal semiconductor quantum wells, also commonly known as nanoplatelets (NPLs), are a new class of atomically flat nanocrystals that are quasi two-dimensional in lateral size with vertical thickness control in atomic precision. These NPLs exhibit highly favorable properties including spectrally narrow photoluminescence (PL) emission, giant oscillator strength transition and negligible inhomogeneous broadening in their emission linewidth at room temperature. Also, as a unique property, NPLs may self-assemble themselves in extremely long chains, making one-dimensional stacks. The resulting excitonic properties of these NPLs are modified to a great extent in such stacked formation. In this thesis, we systematically study the excitonic dynamics of these solution-processed NPLs in stacks and uncover the modification in their excitonic processes as a result of stacking. We have showed that, with increased degree of controlled stacking in NPL dispersions, the PL intensity of the NPL ensemble can be reduced and their PL lifetime is decreased. We also investigated temperature-dependent time-resolved and steady-state emission properties of the nonstacked and completely stacked NPL films, and found that there are major differences between their temperature-dependent excitonic dynamics. While the PL intensity of the nonstacked NPLs increases with decreasing temperature, this behaviour is very limited in stacked NPLs. To account for these observations, we consider Förster resonance energy transfer (FRET) between neighboring NPLs in a stack accompanied with charge trapping sites. We hypothesize that fast FRET within a NPL stack leads increased charge trapping, thereby quenching the PL intensity and reducing the PL lifetime. For a better understanding of the modification in the excitonic properties of NPL stacks, we developed two different models, both of which consider homo-FRET between the NPLs along with occasional charge trapping. The first model is based on the rate equations of the exciton population decay in stacks. The rate equations constructed for each different stack

were solved to successfully estimate the PL lifetime of the stacked ensembles. In the second one, excitonic transitions in a stack are modeled as a Markov chain. Using the transition probability matrices for the NPL stacks, we estimate the PL lifetime and quantum yield of the stacked ensembles. Both models were shown to explain well the experimental results and estimate the observed changes in the excitonic behaviour when the NPLs are stacked. The findings of this thesis work indicate that it is essential to account for the effect of NPL stacking to understand their resulting time resolved and steady-state emission properties.

Keywords: Colloidal quantum wells, semiconductor nanoplatelets, Förster resonance energy transfer, stacking, exciton dynamics.

ÖZET

ÇÖZELTİ HALİNDE İŞLENEN KUANTUM KUYUSU YIĞINLARINDA EKSİTON DİNAMİKLERİNİN ÇALIŞMASI

Onur Erdem
Elektrik-Elektronik Mühendisliği, Yüksek lisans
Tez Danışmanı: Doç. Dr. Hilmi Volkan Demir
Temmuz, 2015

Nanoplakalar (NPL'ler) olarak da bilinen koloidal kuantum kuyuları, kalınlığı atom mertebesinde kontrol edilebilen ve atomik düzeyde pürüzsüz yüzeylere sahip olan iki boyutlu benzeri yeni bir nanokristal türüdür. NPL'ler fotoışıma tayf genişliklerinin çok düşük olması, salınım gücü geçişlerinin çok yüksek olması ve oda sıcaklığında çok az miktarda homojen olmayan ışıma genişlemesine sahip olmaları gibi kullanışlı özelliklere sahiptir. Ayrıca, NPL'ler bir araya gelerek yığın denilen kendilerine özgü, bir boyutlu, çok uzun zincirler oluşturabilirler. Yığılı NPL'lerde eksitonik özellikler yığılı olmayanlara göre büyük ölçüde değişmektedir. Bu tezde, çözelti halinde işlenen NPL yığınlarının eksiton dinamiklerini sistematik olarak inceledik ve yığılma sonucu eksitonik özelliklerinde oluşan değişimleri ortaya çıkardık. NPL çözeltilerinde NPL'lerin yığılması arttıkça, fotoışıma şiddetinin düştüğünü ve fotoışıma ömrünün azaldığını gösterdik. Ayrıca yığılı ve yığılı olmayan NPL filmlerinde eksitonların geçici ve durağan davranışlarını karşılaştırıp sıcaklığa bağlı eksiton dinamiklerinin büyük farklılıklar gösterdiğini gözlemledik. Yığılı olmayan NPL'lerin fotoışıma şiddeti, düşen sıcaklıkla birlikte düzenli olarak artarken, yığılı NPL'lerde bu artış çok düşük düzeydedir. Bu farklılıkları açıklayabilmek için, yığılı NPL'ler arasındaki Förster rezonans enerji transferini (FRET) ve NPL'lerin bazılarında bulunan yük kapanlarını kullandık. Hipotezimiz, NPL yığınlarında çok yüksek hızla gerçekleşmesi beklenen FRET nedeniyle eksitonların çoğunun yük kapanlarında sönümlendiği, bunun sonucunda da fotoışıma şiddetinin ve ömrünün azaldığıdır. Bu hipotezimizin sınanıp NPL'lerin yığınlaşmasının meydana getirdiği değişikliklerin daha iyi anlaşılabilmesi için, hem NPL yığınlarındaki ardışık NPL'ler arasındaki FRET'i, hem de bazı NPL'lerde bulunan yük kapanlarını dikkate alan iki model

geliştirdik. Bu modellerden ilki, NPL yığınlarındaki eksiton miktarının zamana göre değişimini bulmak için diferansiyel denklemler kullanmaktadır. Burada her özgün NPL yığını için oluşturulan diferansiyel denklem sistemlerinin çözümü, yığılı NPL kümelerinin fotoışıma yarıömrünü hesaplamak için kullanılmaktadır. kinci modelde eksitonların NPL yığını içindeki hareketleri Markov zinciri olarak tanımlanmıştır. Burada her bir yığın için oluşturulan geçiş olasılığı matrisleri, fotoışıma ömrünü ve verimliliğini hesaplamada kullanılmıştır. Her iki modelin de deneysel sonuçları açıklayabildiği ve gözlenen sonuçları tahmin edebildiği gösterilmiştir. Bu tezde elde edilen sonuçlar, NPLlerde yığılmanın yarattığı etkinin, NPL'lerin geçici ve durağan ışıma özelliklerini incelenirken hesaba katılmasının gerekliliğini ortaya koymaktadır.

Anahtar sözcükler: Koloidal kuantum kuyuları, yarıiletken nanoplakalar, Förster rezonans enerji transferi, yığınlaşma, eksiton dinamikleri.

Acknowledgement

It has been four years since I first joined the Devices and Sensors Research Group and met the nice people I am happy to be working with. I would like to acknowledge every single one of them for their direct or indirect contributions to my work.

I would like to begin by thanking Prof. Hilmi Volkan Demir for his supervision, guidance and help throughout my research. His continuous motivation and valuable feedback on my work was very helpful in completing this thesis. In addition, I would like to thank Prof. Dönüş Tuncel and Prof. Nihan Kosku Perkgöz for being in my thesis committee, and for their feedback.

I would like to thank Dr. Evren Mutlugün, who took care of me when I joined the group, for introducing me around the lab, showing me experiments for the first time and answering my questions about them. I also thank Dr. Pedro Ludwig Hernández-Martínez for sparing his time to answer my questions patiently. I thank Dr. Emre Sarı for the advices he gave me about the graduate research. I thank Ahmet Fatih Cihan, who assisted me in my final undergraduate semester and the following summer, for his huge effort to help me adopt the group and train me to use most of the tools and instruments that have been crucial in my research, his help and support, and countless Skype meetings to have scientific discussions which proved to be very useful. I thank Burak Güzeltürk for spending hours to explain me stuff, for his mentorship and valuable contribution to my work (and for being the backbone of the unbeaten Haxball team). I thank Dr. Murat Olutaş for the training he gave me on colloidal nanoplatelet synthesis, for providing me with colloidal nanoplatelets over and over and over again and for his contribution to my work (and for not killing me when we were alone in the lab). I thank Kıvanç Güngör for the useful discussion on my research, for his guidance, and his help to run MATLAB simulations. I thank Yusuf Keleştemur for the training he gave me on quantum dot synthesis and providing quantum dots for my research (and for the delicious raw meatballs he made). I thank Talha Erdem for the training he gave me on quantum yield measurement and gold nanoparticle synthesis, and

for helping me achieve constructing a crucial experimental setup for my research. I additionally thank him and Zeliha Soran Erdem for the joyful house parties. I thank Aydan Yeltik for always being helpful and for discussing the same novels again and again, with neither of us remembering we have already done so. I thank Dr. Savaş Delikanlı for the training he gave me on colloidal nanoparticle synthesis, for the nanoplatelets he provided and for trying to scare me in the optical lab (and failing miserably). I thank Shahab Akhavan and Zafer Akgül for the training they gave me on dip coating. I thank Özgün Akyüz for helping me join the group and making sure we never run out of tools and supplements in the lab, Emre Ünal for his huge help on building the sample holder I designed, and Birsen Bilgili for the delicious food she made and all other important arrangements she takes care of.

I thank Dr. Can Uran, Berkay Bozok, Halil Akçalı, İbrahim Akçalı, Somayeh Fardindoost, Dr. Vijay Kumar Sharma and Dr. Manoj Sharma for their friendship and everything I learnt from them. I also thank Onur Akın, Veli Tayfun Kılıç, Sayım Gökyar, Akbar Alipour, Burak Özbey, Sadi Ayhan, Can Usanmaz, Serdarcan Dilbaz and the group alumni I have not already named.

I would like to acknowledge TÜBİTAK for their financial support through BİDEB 2210-A program.

Contents

List of Figures

List of Tables

Chapter 1

Introduction

Colloidal semiconductor nanocrystals (NCs) have been attracting great interest since their introduction. Quantum confinement in these nanoparticles paves the way for the emergence and utilization of new optical properties that are not observed in the bulk form. Modifying the shape and size of the NCs provide control over these new properties, helping to exploit them further. It also creates the opportunity to adjust the electronic structure without having to change chemical composition [1]. Tunability of their size, shape and composition, as well as their free colloidal state allowing them to be integrated into various matrices, make colloidal NCs promising and versatile nanoscale materials [2].

Colloidal NCs of different shapes have been extensively used in a wide variety of applications. In general, the shapes of these nanoparticles can be spherical [3–5], tetrahedral [6], rod-like or tetrapod-like [7]. To date, these NCs have been used in applications including light-emitting diodes (LEDs) [8, 9], lasing [10], solar cells [11] and transistors [12]. Properties of these NCs such as increased photostability compared to their organic counterparts [13] and high absorption cross-section despite their small size [14] make colloidal semiconductor NCs favorable for these applications.

The most recent type of colloidal nanocrystals introduced in the literature is

the colloidal quantum wells, commonly dubbed nanoplatelets (NPLs). Colloidal NPLs are quasi two-dimensional nanocrystals with controllable thickness in atomic precision [15, 16]. Typically, due to wide lateral dimensions, quantum confinement is only in one-dimension. Very narrow photoluminescence emission linewidth, giant oscillator strength transition and fast radiative exciton recombination are among the favorable properties of NPLs [16, 17].

Semiconductor nanocrystals can be coupled to each other or other types of nanoparticles in order to further alter their electrooptical properties thanks to the interaction between the electronic excitation states in these particles. For instance, plasmonically coupled semiconductor NCs and metal nanoparticles are used to enhance fluorescence of the NCs or obtain polarized emission from the isotropic quantum dots (QDs) [18–20]. Another widely utilized interaction is Förster resonance energy transfer (FRET), which is a nonradiative process to transfer excitations from one emitter to another in resonance [21]. FRET takes place not only between semiconductor NCs but also in organic chromophores such as dyes and fluorescent proteins. It is extensively used in biosensing and bioimaging applications. Soon after stable colloidal NCs were developed, FRET started to be exploited in these materials as well. Efficient FRET between QDs of different sizes has been demonstrated [22]. QDs have also been integrated into biological applications involving FRET. Energy transfer of QDs have been used in biosensing and biolabeling applications [23, 24]. Efficient FRET has been observed between QDs and dye-labeled proteins or dyes attached to DNA moleculues [25, 26]. This is useful especially for the applications of distance measurement based on the strength of FRET, which is highly sensitive to the distance between the particle that transfers the excitation (donor) and the one that receives it (acceptor).

FRET is expected to be observed not only for isolated donor-acceptor pairs but also for large particle clusters. For example, FRET in close-packed QDs leads to a red shift in steady-state photoluminescence emission spectrum, along with slower fluorescence decay in the red tail of the emission feature and faster decay in the blue tail due to the tendency of excitons to transfer from QDs having wider bandgaps towards those having narrower bandgaps [27]. Similar trends

in steady-state PL have been observed in QD aggregates as well [28]. In such nanoparticle aggregates, FRET rates are expected to be higher due to the small seperation between the fluorophores.

Similar to QD aggregates, colloidal NPLs have also been observed to have a unique self-assembly formation [29]. These self-assembled NPL chains are regarded as stacks. Stacked NPLs stand in a face to face orientation, and come so close to each other that their capping ligands are expected to get interlocked [30]. A NPL stack can contain hundreds of NPLs and form one-dimensional superlattices that can be several micrometers long [29].

So far, studies on self-assembled NPLs have been quite limited. NPL stacks were shown to emit polarized light due to their highly anisotropic nature [29]. A recent study demonstrated biexciton transfer within a NPL stack at a high rate [31]. In a recent report by our group, transient and steady-state exciton dynamics in NPL ensembles with controlled stacking have been studied [32]. This work revealed that increased degree of stacking in NPL ensembles reduces the exciton decay lifetime as well as the PL intensity. Although there are extensive studies and theoretical explanations for the modifications in the excitonic dynamics of fluorophores like QDs and fluorescent dyes, the underlying physics causing the changes in the excitonic behaviour in the NPL stacks are not well understood.

In this thesis, we propose two different models to explain the reduction in lifetime and PL intensity of the NPLs, when they are in stacked form. The first one uses rate equations to solve for the exciton population decay in partially stacked NPL ensembles to estimate the decay times. The second one regards excitonic transitions in a stack as a Markovian process, and calculates the changes in both the PL lifetime and intensity of the stacked NPLs as a function of temperature. Estimations using these models have been compared with our experimental data in the respective studies.

The thesis begins with an overview on colloidal NPLs in Chapter 2. Here, the synthesis procedure is described and the optical properties of the NPLs are explained. This is followed by a brief introduction to nonradiative energy transfer

(NRET) and its dynamics. Chapter 3 is based on the publication of Guzelturk et al. on the change of excitonic properties of the CdSe NPLs as a function of the degree of stacking in the ensemble [32] and the contribution of this thesis work in particular on the development of a model based on the rate equations. This model is used to explain the fluorescence lifetime shortening when stacking is introduced and it is derived and explained in detail. In Chapter 4, temperature-dependent transient and steady-state photoluminescence in nonstacked and fully stacked NPL ensembles are compared, and the differences are explained using a new model developed using Markovian processes. This model is able to estimate both the PL lifetime and QY. This piece of the thesis work is submitted for a peer-reviewed journal publication. Chapter 5 concludes the thesis with final remarks on the importance of the obtained results and future work.

Chapter 2

Scientific Background

2.1 An overview of nanoplatelets

Colloidal semiconductor quantum wells (QWs), also known as nanoplatelets (NPLs) are a type of atomically flat, quasi-two dimensional (2D) nanocrystals that have been introduced very recently to the literature. While these 2D nanostructures have typically only few monolayers (MLs), making 1-3 nm in vertical thickness, they have lateral sizes on the order of 10 nm [16, 30, 33], which is larger than the exciton Bohr radius. Therefore, the quantum confinement effect is observed strongly in the tight vertical dimension. The optical properties of NPLs are thus mainly determined by their vertical thicknesses. For instance, the spectral location of absorption and emission features shift from 3.1 down to 2 eV, when the thickness of the NPLs increases from 1.22 to 2.13 nm [16]. Therefore, similar to color tuning in spherical nanocrystal quantum dots (QDs), the thickness of the NPL provides tunability of the bandgap emission. The lateral dimensions are almost ineffective in determining the spectral properties as long as they are longer than the exciton Bohr radius of the material. They do, however, change properties such as extinction coefficient, photoluminescence quantum yield (QY) and exciton lifetime [34].

2.1.1 Colloidal synthesis of nanoplatelets

For a typical synthesis of CdSe NPLs, cadmium myristate as Cd precursor and elemental selenium as Se precursor are dissolved in octadecene (ODE) [15]. The solution is placed into a three-neck flask, degassed for 10 to 30 min [15, 29, 35], and then heated up. When the temperature is around 200 C, a cadmium acetate salt is introduced into the flask to induce the lateral growth [15]. For 4 ML CdSe synthesis, the solution is heated up to and kept at 240 C for 4-10 min [32, 35, 36]. After the system is cooled down to room temperature, oleic acid is added to the solution to be used as ligand and increase solubility [29, 32, 36, 37]. Final reaction product can contain unstable nanoparticles that did not exhibit lateral growth as well as NPLs with different thicknesses. The desired type of nanoparticles can be separated from the others using selective precipitation techniques. NPLs are typically dissolved in hexane [17, 32, 33, 38–40].

Figure 2.1 displays high-angle annular dark field (HAADF) transmission electron microscopy (TEM) images of 4 ML CdSe NPLs. Here, NPLs are lying flat on the surface. The uniformity of gray tones indicates that all the NPLs have the same thickness. The absorbance and photoluminescence (PL) spectra of 4 ML CdSe NPLs are shown in Figure 2.2. There are two features at 480 and 512 nm of the absorption spectrum, which correspond to electron-light hole and electron-heavy hole transitions, respectively. The peak of the PL emission is at 514 nm with a full-width at half maximum of 9 nm ($\sim$42 meV) at room temperature. As can be seen in the figure, the Stokes shift between the absorption and emission spectra is very small. This is also the characteristics of NPLs with different vertical thicknesses [16, 41].

NPLs exhibit the appealing properties of atomically flat surfaces and narrow PL emission. These properties have already started to be utilized in applications including light-emitting diodes (LEDs) [42] and optically pumped lasers [38, 43]. Moreover, the advanced core/shell structure of NPLs similar to the QDs, as well as core/crown structure unique to NPLs allow these properties to be further exploited. In the core/shell architecture, a second type of semiconductor is grown

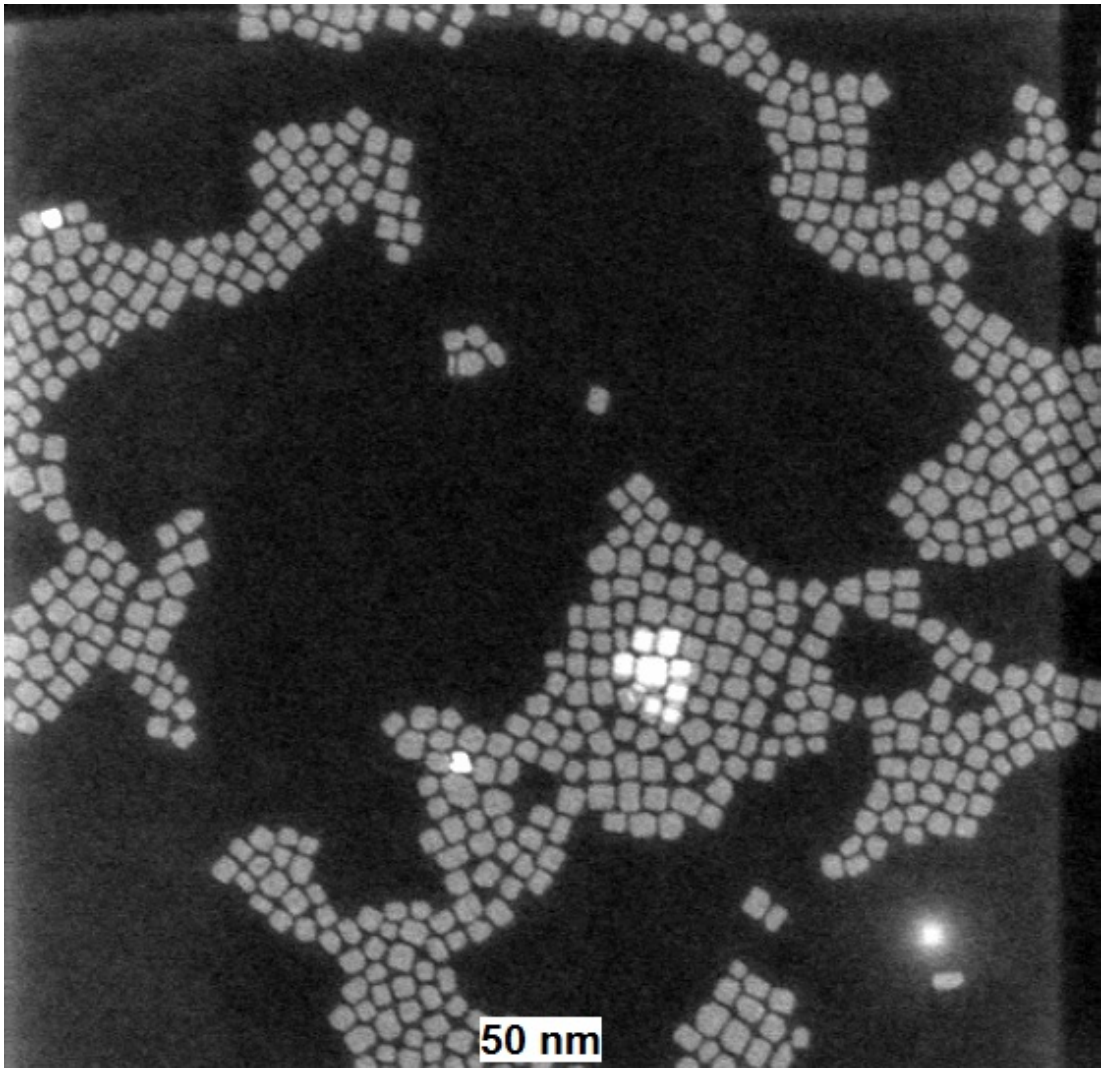

Figure 2.1: HAADF-TEM images of 4 ML CdSe NPLs.

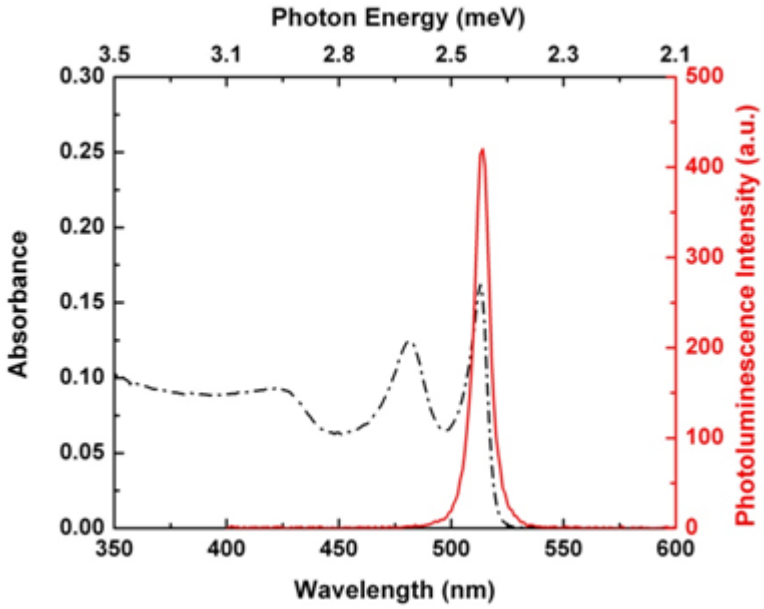

Figure 2.2: Absorbance (dot-dashed line) and PL emission (solid line) of 4 ML CdSe NPLs.

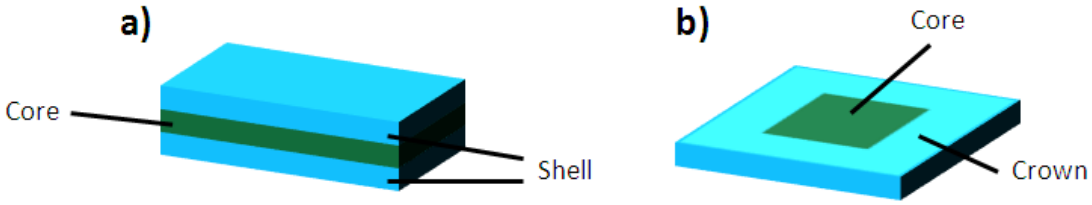

Figure 2.3: Schematic representations of a) core/shell and b) core/crown heteronanoplatelets.

vertically on the planar surfaces of the starting core semiconductor. When the extension of the second type of semiconductor is in lateral directions, the resulting structure leads to core/crown architecture. Figure 2.3 schematically demonstrates these two heterostructures. Shell coating on NPLs enables higher quantum yield (QY) as a result of efficient surface passivation [33, 44, 45]. The core/crown NPLs have been utilized for efficient exciton transfer from the crown to the core and continuous bandgap tunability [46–49].

2.1.2 Self-assembly of nanoplatelets

As discussed previously, colloidal NPLs are expected to lie flat on a planar substrate, as seen in Figure 2.1. However, NPLs may also assemble together, forming long NPL chains. This phenomenon is commonly regarded as stacking. When the NPLs are stacked, they become facially aligned with each other with a very small separation distance between them. The TEM imaging of a stacked CdSe NPL ensemble is shown in Figure 2.4. In contrast to nonstacked NPLs, which are lying flat on the TEM grid, the stacked NPLs stand perpendicular to the grid. This face-to-face aligned orientation of NPLs in a stack allows the neighboring NPLs to come very close to each other and create a very dense solid film. The reported values for interspacing between the CdSe NPLs with 4 MLs of thickness vary between 4 and 5 nm [29, 30, 32].

To induce stacking formation, two methods have been proposed so far. The first one is the evaporation of the solvent, which causes aggregation of the NPLs on a planar surface (e.g., TEM grid, glass substrate) [30]. The second is the addition of a polar solvent, e.g. ethanol, to the NPL solution [29]. The formation of the stacked NPL chains after the addition of ethanol is explained by the fact that ethanol is a weak solvent for the surfactant oleic acid. With more ethanol added to the solution, oleic acid molecules will be forced away from the ethanol and close interaction between two oleic acid molecules will be more and more favoured and attractive forces (e.g. van der Waals) between close pairs of NPLs will be effective [29]. As a result, addition of the ethanol will induce stacking in NPLs. Ethanol is also used for controlled stacking of NPLs in a previous study of our group [32]. It is clearly observed that, as the amount of ethanol added to the dispersion increases, the degree of stacking in the ensemble is also increasing, as seen in Figure 3.2.

When the NPLs are in the stacked configuration, their optical properties differ from the nonstacked NPLs. Studies with the stacked NPL ensembles reveal that the micrometer-long NPL assemblies emit polarized light [29]. Temperature-dependent steady-state spectroscopy of the stacked NPLs indicate a second PL

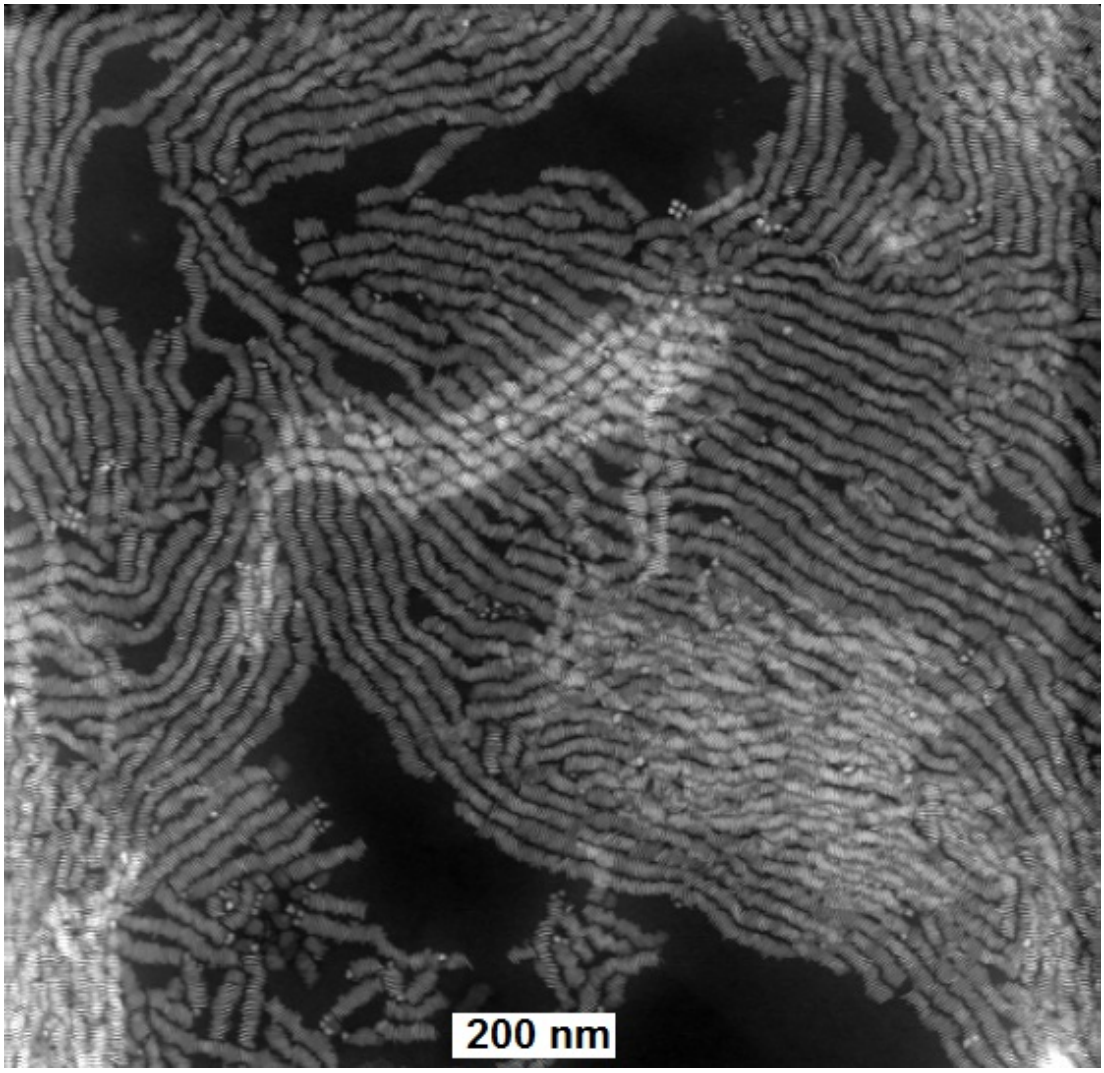

Figure 2.4: TEM imaging of stacked 4 ML CdSe ensemble

peak at low temperatures, which is slightly red-shifted [30]. In a more recent study, biexciton transfer within the NPLs of a stack has been demonstrated [31]. Our study revealed that, with the increased degree of stacking, we observe PL intensity quenching as well as faster transient PL decays [32].

Stacking in NPLs possibly paves the way for emergence of new electronic and optical features by forming superparticles in the form of one-dimensional superlattices. Stacks allow NPLs to stay in very close proximity to each other, which is expected to create extraordinarily strong excitonic interaction between them. This aspect will be studied and discussed in detail in the following section and chapters.

2.2 Nonradiative energy transfer

Excitation energy in a fluorophore molecule or particle can be transferred to another fluorophore nearby without the emission of a photon. In this case, the former one reduces to its ground state and the latter raises to an excited state. This phenomenon is referred to as nonradiative energy transfer (NRET). In the energy transfer, the fluorophore that transfers its excitation is regarded as the donor, and the one that is excited via NRET as the acceptor. Figure 2.5 schematically demonstrates an example of NRET from the donor to the acceptor. This schematic illustrates a donor with an electron-hole pair initially at the first excited state and an acceptor with a resonant state with the excitation in the donor. In this case, the excitation can be transferred to the acceptor via NRET. The electron-hole pair in the acceptor recombines, and an electron-hole pair with the same energy is created in the acceptor. The resulting exciton in the acceptor quickly relaxes to the band edge, and then finally recombines. As a result, if this recombination is a radiative process, a photon is emitted from the acceptor.

In general, the acceptor does not have to be luminescent; so, the emission of the photon from the acceptor after the energy transfer is not necessary. However, for most practical applications, luminescent acceptor molecules or particles are

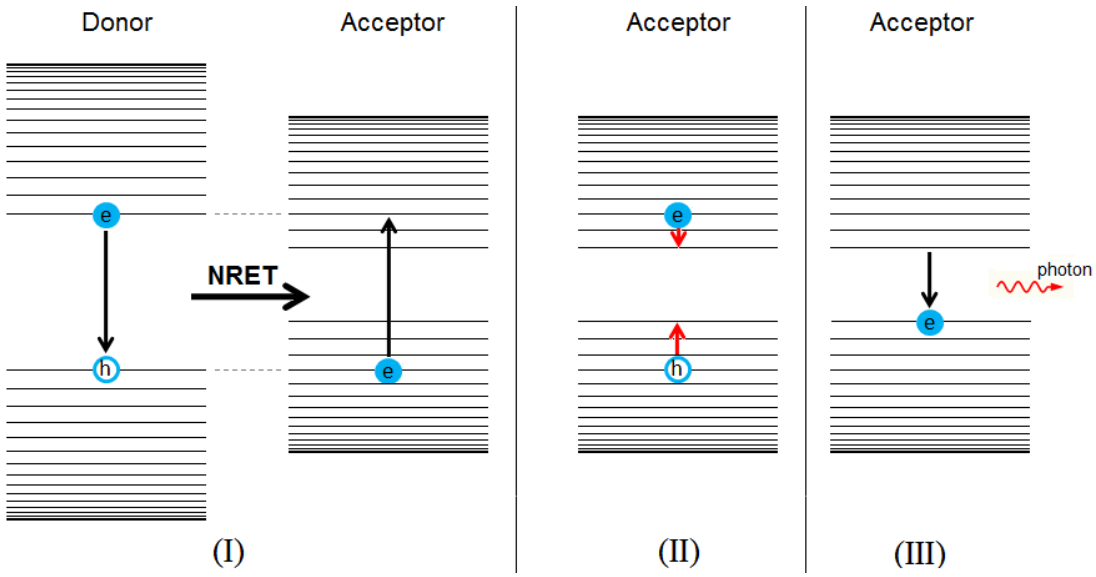

Figure 2.5: Schematic representation of NRET from a donor to an acceptor: (I) Donor in the first excited state transfers its energy via NRET to the acceptor in the ground state. (II) Excited acceptor molecule quickly relaxes to the first excited state. (III) First excited state of the acceptor decays to the ground state and a photon is emitted.

used. In the case of luminescent acceptors, emission of the photon always comes from the transition from the lowest unoccupied molecular orbital (LUMO) to the highest occupied molecular orbital (HOMO) because the relaxation of the electron (hole) to LUMO (HOMO) happens via thermalization at a much faster rate than the radiative recombination. In case of nonmolecular materials, this corresponds to the relaxation to the band edge before the recombination. Similarly, if the donor is excited to an energy level higher than band edge, the energy is still transferred from the band edge due to very high rate of hot carrier relaxation compared to the rate of the energy transfer.

From the illustration of NRET in Figure 2.5, a necessary condition for NRET is that there should be a state in the acceptor resonant to the state of the excitation in the donor. Otherwise, the excitation cannot be transferred to the acceptor. In terms of optical processes, this condition translates to the requirement that there should be nonzero overlap between the emission spectrum of the donor and absorption spectrum of the acceptor. Another necessity for the energy transfer is that transition dipoles of donor and acceptor states should be oriented properly

with respect each other to allow energy transfer and the donor and acceptor pair should be physically close to facilitate strong enough electromagnetic dipole-dipole coupling.

The first successful attempt to understand the underlying physics of NRET was made by Theodore Förster. He correctly estimated that there should be a spectral overlap of the donor's emission and acceptorSs absorption spectra as well as the non-zero dipole orientation factor in order for the donor to transfer its energy to an acceptor nonradiatively [50]. The root cause of this interaction between the donor and the acceptor is the electric field caused by the transient dipole of the electron-hole pair in the donor, which acts as a point dipole. Förster's theory, which he proposed and developed in 1940?s, is still widely used today. Therefore, NRET is also commonly referred to as Förster resonance energy transfer (FRET).

2.2.1 Förster theory

According to Förster's formulation, the rate of NRET from the donor to acceptor is determined by [21]

$$\gamma_{NRET} = \frac{1}{\tau_D}\left(\frac{R_0}{R}\right)^6 \tag{2.1}$$

where τ_D is the recombination lifetime of the excitation in the absence of the donor, R is the distance between the donor and the acceptor, and R_0 is the Förster radius defined by

$$R_0 = \left(\frac{9000ln(10)\kappa^2 Q_D}{128\pi^5 N_A n^4}\int_0^\infty F'_D(\lambda)\epsilon_A(\lambda)\lambda^4 d\lambda\right)^{1/6} \tag{2.2}$$

In this expression, κ^2 is the dipole-dipole orientation factor, Q_D is the quantum yield (QY) of the donor in the absence of the acceptor, N_A is Avogadro's number, and n is the refractive index of the environment. The integral expression

is the overlap in between the absorbance of the acceptor, $\epsilon_A(\lambda)$, and the normalized emission intensity of the donor, $F'_D(\lambda)$. The overlap integral J can be reformulated as [51]

$$J = \int_0^\infty F'_D(\lambda)\epsilon_A(\lambda)\lambda^4 d\lambda = \frac{\int_0^\infty F_D(\lambda)\epsilon_A(\lambda)\lambda^4 d\lambda}{\int_0^\infty F_D(\lambda)d\lambda} \tag{2.3}$$

where $F_D(\lambda)$ is donor's emission spectrum with arbitrary units. Expressing J this way removes the necessity to normalize the emission spectrum.

It can be deduced that NRET creates a new channel for the excitation decay in the donor. The first decay channel is the recombination of the exciton in the donor, which can be radiative or nonradiative. The new channel is the nonradiative transfer of excitation energy to the acceptor. The two different processes compete with each other, which in turn alters the transient excitonic dynamics in the donor. It can be shown that the exciton lifetime of the donor in the presence of acceptor is

$$\tau_{DA} = \frac{1}{\left(\gamma_{NRET} + \frac{1}{\tau_D}\right)} \tag{2.4}$$

Defining $\gamma_D = 1/\tau_D$ as the donor's initial exciton recombination rate in the absence of an acceptor, the efficiency of NRET is

$$\varepsilon_{NRET} = \frac{\gamma_{NRET}}{\gamma_{FRET} + \gamma_D} \tag{2.5}$$

Using the expression for γ_{NRET} in Eq. 2.1, we obtain

$$\varepsilon_{NRET} = \frac{\left(\frac{R_0}{R}\right)^6}{\left(\frac{R_0}{R}\right)^6 + 1} \tag{2.6}$$

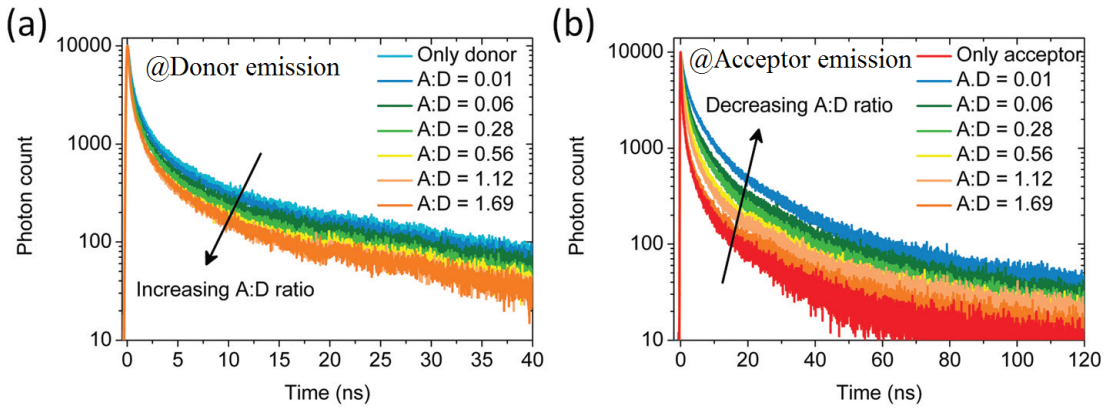

Figure 2.6: Acceptor and donor photoluminescence decays for donor-acceptor combinations of different ratios. Donor and acceptor fluorophores are 4 ML and 5 ML CdSe NPLs, respectively. Reprinted by permission from [52].

Hence, the Förster radius R_0 is the distance that makes the NRET efficiency 50%. NRET efficiency can be extracted from the time-resolved fluorescence (TRF) measurements. After determining τ_D and τ_{DA}, the NRET efficiency can be calculated by

$$\varepsilon_{NRET} = 1 - \frac{\tau_{DA}}{\tau_D} \tag{2.7}$$

NRET from the donor to the acceptor alters the excitonic dynamics in the donor and the acceptor by transfering excitons from the donor to the acceptor. As stated above, the modified exciton decay lifetime in the donors when the NRET is effective is given by Eq. 2.4. τ_{DA} is shorter than τ_D as expected.

Similarly, the exciton decay lifetime of the acceptor in the presence of a donor, τ_{AD}, is different than the decay time in the absence of the donor, τ_A. τ_{AD} is expected to be larger than τ_A because of the extra excitons fed from the donor. An exemplary evolution trend of donor and acceptor fluorescence decays for different donor:acceptor NPL ratios are shown in Fig. 2.6. With more acceptors added, the PL decays of the excited donors get faster. On the other hand, when there are more donors to feed each acceptor, the decay time of the acceptor emission increases.

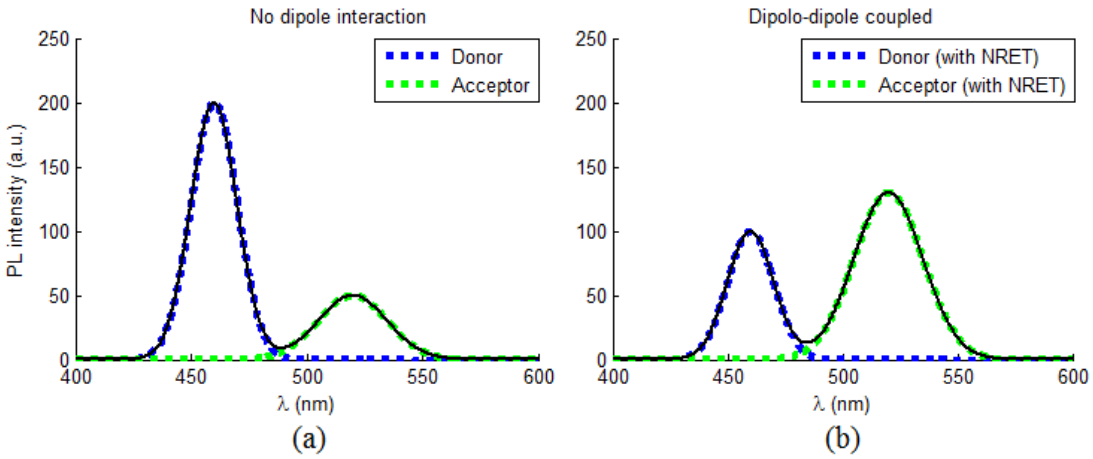

Figure 2.7: Hypothetical PL spectra of donor and acceptor ensembles without (left) and with FRET in between them. Dashed blue (green) line is donor (acceptor) emission spectrum. Solid black line is the total emission spectrum.

Concomitantly, the steady-state PL intensities of the donor and acceptor fluorophores also change as a result of NRET. With some of the excitons in the donor species being transferred to the acceptor, the PL intensity of the donor decreases when the donors are coupled to the acceptors. Fluorescent acceptors, on the other hand, will have higher PL intensity due to the additional excitation via NRET. Figure 2.7 illustrates this situation: When the donors and acceptors are not coupled to each other with no NRET between them, they will have their own emission spectra, neither of them affecting each other. When the donor and acceptor species interact and transfer energy via NRET, the shape of the final emission spectrum will change. The intensity coming from the donor will decrease whereas the intensity of the acceptor emission will increase. The decrease in the donor PL intensity and the increase in the acceptor PL intensity due to NRET has been widely observed previously, e.g. for CdSe/ZnS core/shell QD donors and protein molecules labeled with Cy3 dye acceptors [25].

NRET is extensively used in many different applications today, including making DNA analyses [53], imaging proteins [54] and increasing quantum yield of nanocrystal structures [55]. NRET can also be used for determining distance between the donors and acceptors in an ensemble as a nano-ruler. In fact, for a specific donor-acceptor pair for which the Förster radius is known, Eq. 2.7 can be used to determine the FRET efficiency, and thereby the distance between the

donor-acceptor pairs. Of course, this simplistic approach works well when the donor species have single exponential decays, the distance between each donor-acceptor pair is the same, and each donor is coupled to only one acceptor, and vice versa. None of these conditions are likely to occur in an ensemble composed of billions of molecules or particles. In the case of a multiexponential decay, amplitude-averaged lifetime is used [51]. More complex analysis is required in the case that the donor-acceptor spacing is variant [56, 57]. Nevertheless, Eq. 2.7 still gives an estimation of average donor-acceptor seperation.

2.2.2 Bidirectional energy transfer

One of the requirements for NRET from one fluorophore to the other, as discussed, is that there should be a non-zero spectral overlap between the emission of the former fluorophore and the absorption of the other. If there is also an overlap between the absorbance spectrum of the first fluorophore and the emission spectra of the other, NRET in the reverse direction is also possible, and thus both species can transfer excitations to each other. Bidirectional energy transfer is commonly seen in NRET between the same type of nanoparticles, known as the homo-NRET. Homo-NRET was previously observed for the QD populations of similar sizes, therefore having bandgaps close to each other. It was found that in this case the overall emission spectrum red-shifts in the presence of NRET [22, 27]. This can be explained using the hypothetical QD ensemble shown in Figure 2.8: There are three different QD subclasses with the corresponding bandgap energies E_1, E_2 and E_3 such that $E_1 > E_2 > E_3$. The QDs with the higher bandgap energy are expected to transfer energy at a higher rate because their spectral overlap J with any other QD is larger than those with the other two QD populations. Therefore, the rate of energy transfer from the wider bandgap QDs to the narrower bandgap QDs is larger than the rate of energy transfer in the reverse direction. This eventually causes more of the excitations to end up in the QDs with smallest bandgap energies. As a result, those QDs that are on the red tail of the overall emission spectrum on the ensemble have increased emission intensity, whereas the dots on the blue tail emit fewer photons, since they transfer energy with a

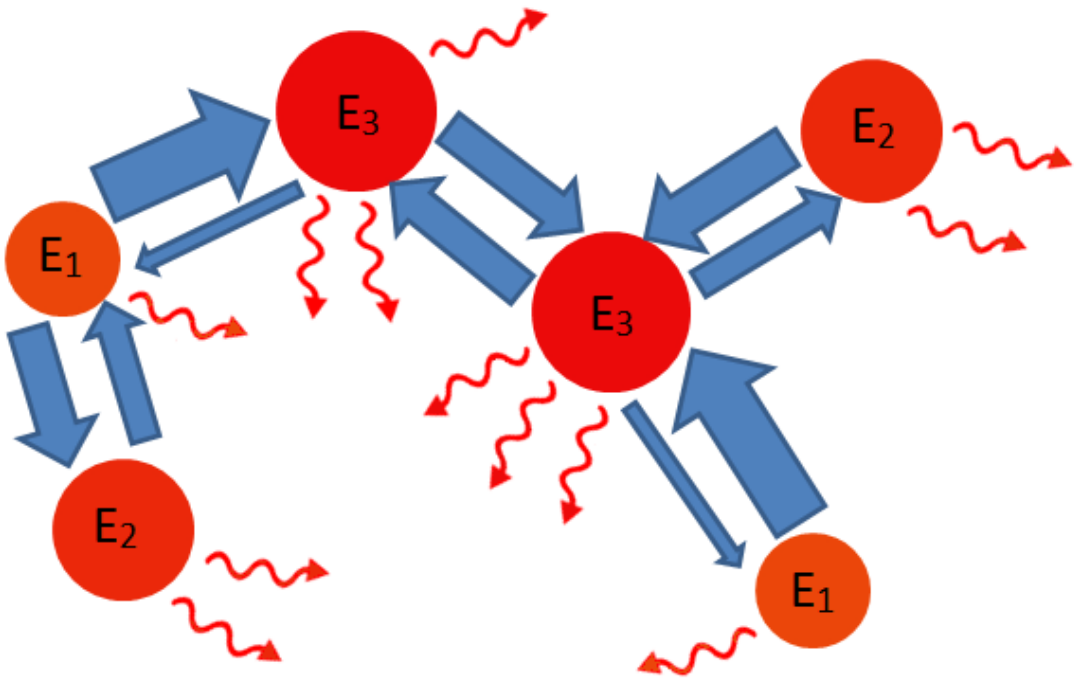

Figure 2.8: Reciprocal energy transfer between close-packed QDs with different NRET rates. Excitations tend to go to the narrower bandgap energy QDs, resulting in increased emission from them and an overall red-shifted emission spectrum for this QD ensemble.

rate faster than those of the narrower bandgap QDs. Another result of the NRET between these QDs is that the excitation decay is quicker on the blue tail whereas it typically slows down on the red tail [25].

These modifications in the transient and steady-state excitonic dynamics of this QD ensemble is a result of inhomogeneous broadening due to size variations, which is practically inevitable for colloidal QDs. The colloidal NPLs, however, have magic-sized thicknesses, and are expected to have very little inhomogeneous broadening. In fact, temperature-dependent spectroscopy of single NPLs revealed that the broadening in NPLs are homogeneous [17]. Therefore, the transient and steady-state behaviour of close-packed NPL assemblies (i.e., NPL stacks) might differ from those of these QDs. To understand the associated underlying physics and explain its impact, Chapters 3 and 4 will study the homo-NRET between the NPLs in stacks, which is expected to take place at a very high rate and have excitons to resonate over longer distances in each NPL chain.

Chapter 3

Time-resolved optical spectroscopy study and photoluminescence lifetime estimation of stacked nanoplatelets using rate equations

Our first approach to understand the change in the photoluminescence decay kinetics of nanoplatelets with stacking is the use of rate equations to find the fractional number of excitons in each site of a particular stack as a function of time. This approach is used in the study by Guzelturk et al., in which the NPL ensembles were partially stacked to different extents [32]. In this work, the transient and steady-state excitonic processes with different degrees of stacking were studied and it was observed that, as NPLs form into stacks, the photoluminescence quantum yield is quenched and the transient exciton decay is accelerated. We show that stacking in colloidal NPLs substantially increases the exciton transfer

and trapping in the NPL chain. The efficiency of Förster resonance energy transfer within the stacks can be surprisingly as high as 99.9%, with an estimated extraordinary Förster radius as long as 13.5 nm. Long-range NRET therefore boosts exciton trapping in nonemissive NPL subpopulation, thereby quenching photoluminescence when the NPLs are stacked. A theoretical model based on exciton decay rate equations has been developed to explain the effect of stacking on photoluminescence intensity and transient decay. The estimated decay lifetimes using the model show excellent match with the experimental data. This chapter is partially taken from our SCI journal publication in ACS Nano [32], in which the author of this thesis is a co-author and the rate equations model has been developed by this thesis' author.

3.1 Experiment

3.1.1 Sample preparation

The 4 ML CdSe nanoplatelets (NPLs) were synthesized using a modified recipe from Ref. [15]. 170 mg of cadmium myristate, 12 mg of selenium and 15 mL of octadecene were loaded into a three-neck flask. After evacuation of the solution at room temperature, the solution was heated up to 240 °C under argon atmosphere. When the color of the mixture solution turned yellowish around 195 °C, 45 mg of cadmium acetate dehydrate was introduced. After 4 min of growth, the reaction was stopped and cooled down to room temperature, and 1 mL of oleic acid was injected into the solution. The setup for the NPL synthesis is shown in Figure 3.1. Successive purification steps were used to separate 4 ML CdSe NPLs from other reaction products.

For the time-resolved fluorescence (TRF) measurements, 3 mL of the NPL solution in hexane was filled into a quartz cuvette. The degree of stacking was controlled by the addition of ethanol into the NPL dispersion in hexane. Ethanol is known to initiate stacking in NPLs [29]. To increase the degree of stacking,

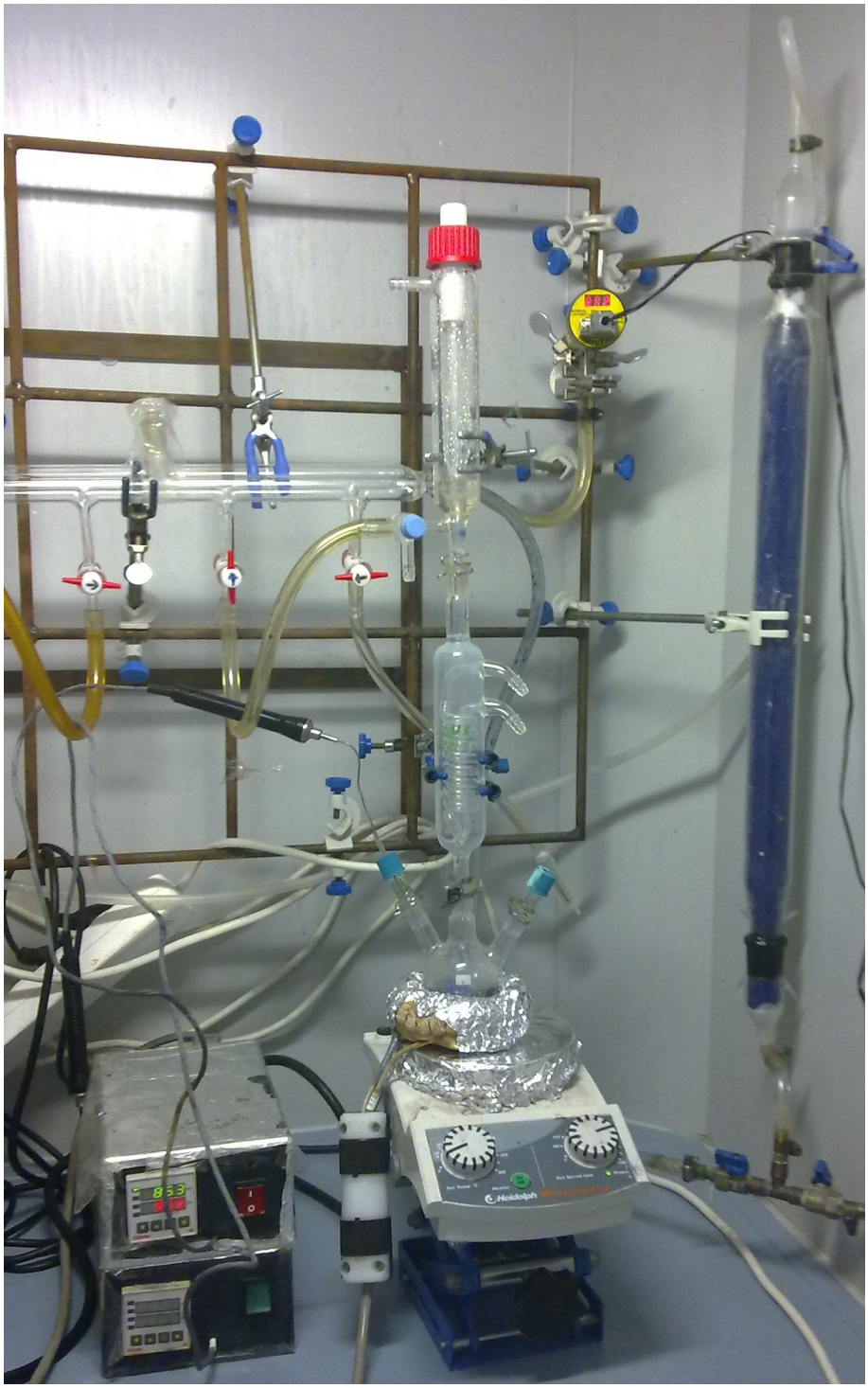

Figure 3.1: Our NPL synthesis setup in a fume hood consisting of a three neck flask, a temperature controller, a pressure gauge and a Schlenk line at our Bilkent UNAM laboratory.

we added more ethanol to the same NPL dispersion. The TEM image of NPLs with no observable stacking at all is shown in Figure 3.2(a). As can be seen in the figure, the NPLs are lying flat on the TEM grid, they are well seperated and there is no indication of stacking. Figures 3.2(b), 3.2(c) and 3.2(d) show the TEM imaging of NPL ensembles after 55, 135 and 455 µL of ethanol was added to the same NPL solution, respectively. As the amount of ethanol increases, more of the NPLs are assembled into stacks and the existing stacks get longer. Figure 3.3 shows the measured distribution of stack sizes in the three partially stacked ensembles as a means of the number of NPLs in the stacks.

3.1.2 Experimental setup

To study the time-resolved fluorescence of the NPL ensembles, we used FluoTime 300 time-resolved spectrometer and PicoHarp 200 time-correlated single photon counting (TCSPC) unit. The system, shown in Figure 3.4, is composed of an excitation laser at 375 nm, a monochromator, a photomultiplier tube (PMT), and a laser control unit. The pulsed laser beam hits the sample at a repetition rate of 2.5 MHz. The PL decays were taken at the peak emission wavelength.

3.1.3 Results and discussion

We studied the transient and steady-state optical properties of the described stacked NPL ensembles via time-resolved fluorescence and steady-state photoluminescence measurements. The photoluminescence decay curves are shown in Figure 3.5(a) together with their numerical fits. It can be seen that, as more ethanol was added to the solution, i.e., the degree of stacking was increased, the decay time got shorter. Steady-state photoluminescence spectra of the same samples are shown in Figure 3.5(b). Here, photoluminescence intensity decreases with the increased stacking. With the most stacked case, in which 455 µL of ethanol was added to the NPL solution, the intensity decreased to about a tenth of the completely nonstacked case. Black dots in Figure 3.5(c) depicts

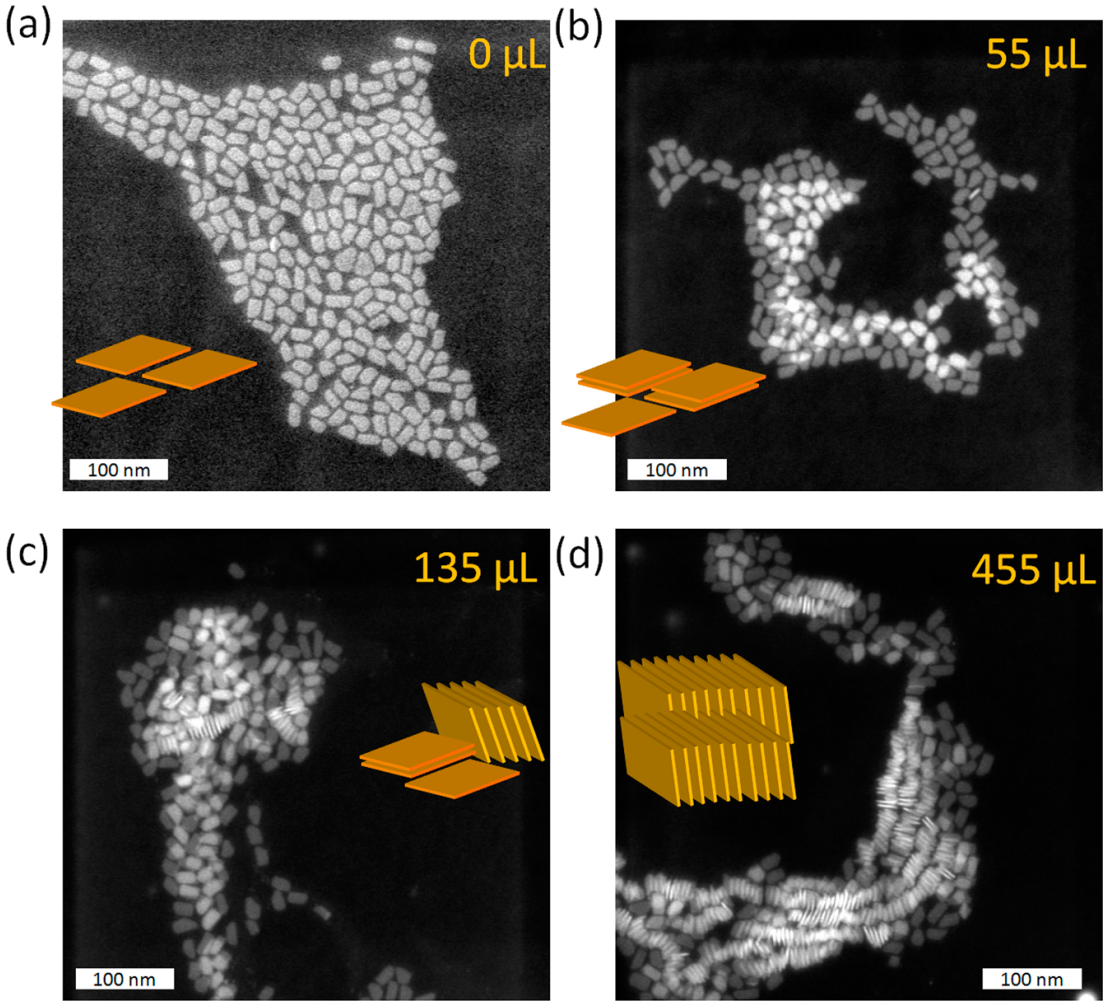

Figure 3.2: HAADF TEM images of the NPLs with (a) no ethanol and a total of (b) 55 µL, (c) 135 µL, and (d) 455 µL of ethanol added. As the total added ethanol amount is increased gradually, longer column-like stacks of the NPLs are formed. On each image, a cartoon-like illustration of the evolution of the stacking in NPLs is presented by yellow-colored NPLs. Reprinted from [32] with copyright permission from ACS.

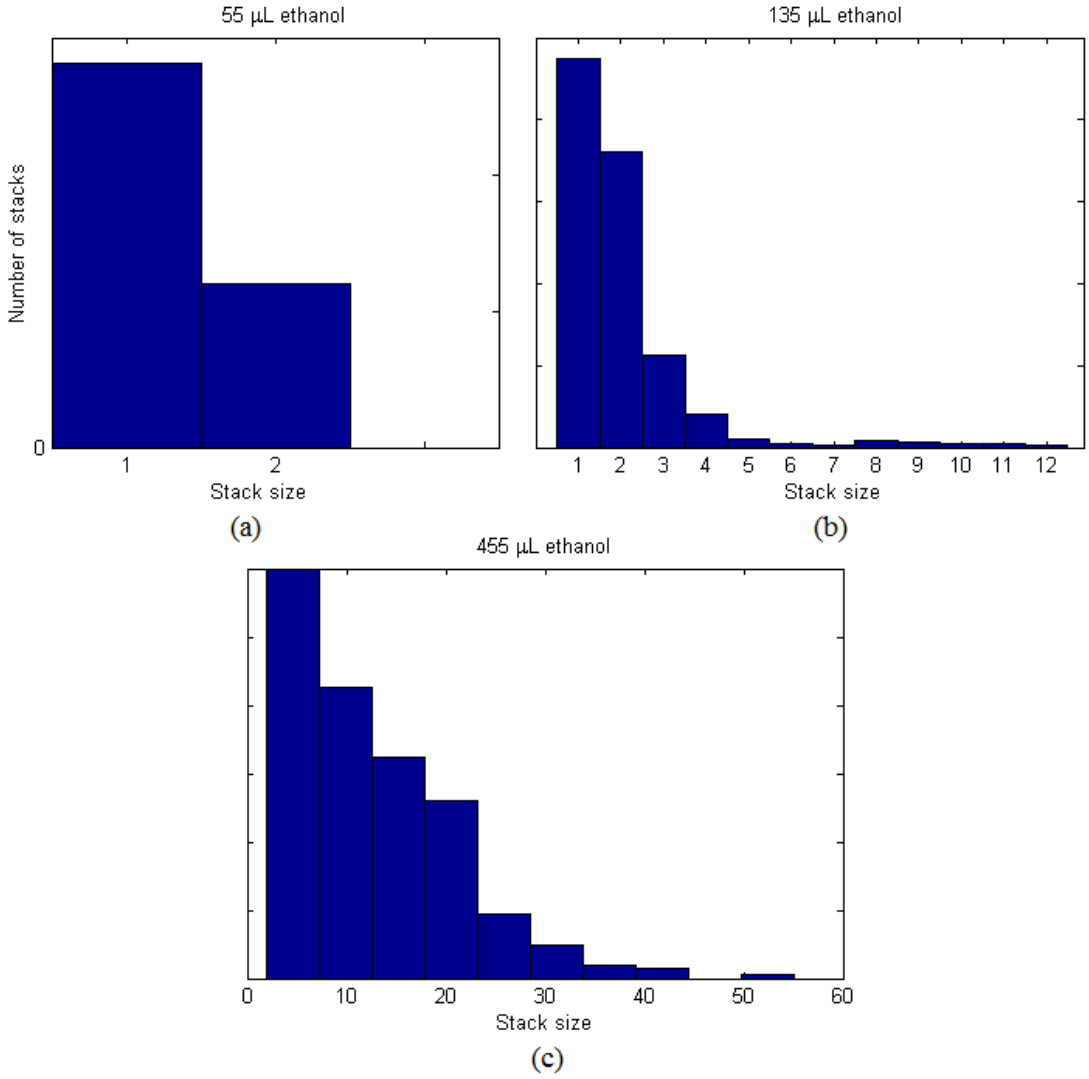

Figure 3.3: Distribution of the stack size for the NPL dispersion mixed with (a) 55 µL, (b) 135 µL and (c) 455 µL ethanol. Reprinted from Supplementary Information of [32] with copyright permission from ACS.

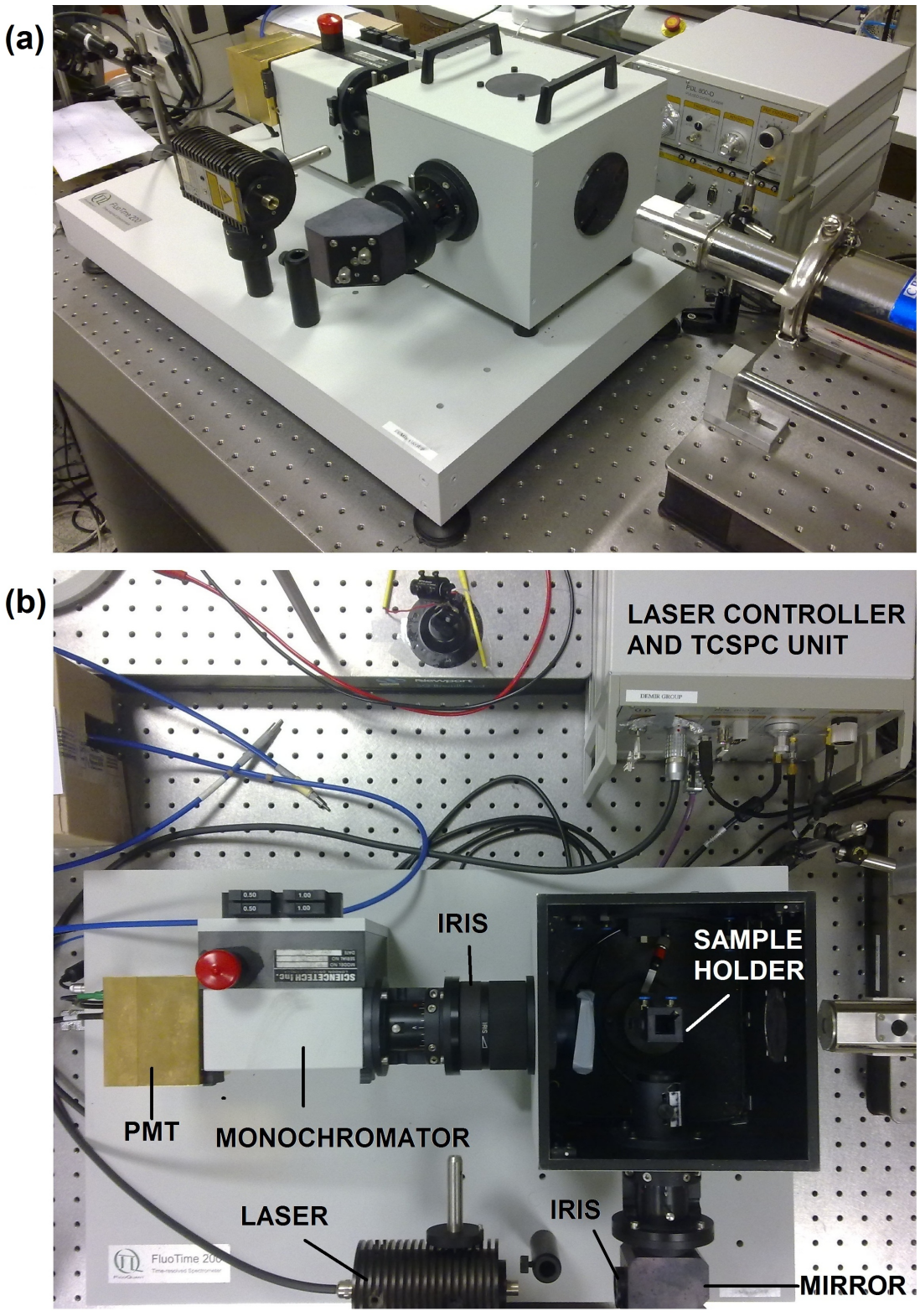

Figure 3.4: (a) Our FluoTime 200 time-resolved spectrometer setup at our Bilkent UNAM laboratory. (b) The same experimental setup from the top view. The cover of the sample chamber is removed to reveal the sample holder.

the amplitude-averaged photoluminescence lifetimes of the NPLs as a function of the total amount of ethanol added. The amplitude-averaged lifetime is 3.38 ns before stacking is initiated, and it reduces down to 0.3 ns when 455 µL of ethanol is added. Finally, the photoluminescence quantum yield of the NPL ensembles as a function of the added ethanol amount is presented in Figure 3.5(d). The QY of nonstacked ensemble was measured to be 30.3% by comparing its emission intensity with a rhodamine 6G reference dye, which has a QY of 95.0%. Using

$$QY = \frac{\gamma_r}{\gamma_{total}} \tag{3.1}$$

where γ_r is the radiative recombination rate of NPLs, $\gamma_{total} = 1/\tau_{total}$ is the total (radiative and nonradiative) recombination rate of NPLs and $\tau_{total} = 3.38$ ns when there is no stacking, we get $\gamma_{rad} = 0.090$ ns^{-1}. Assuming the radiative rate does not change with the amount of ethanol in solution, we can calculate the photoluminescence QY by using Eq. 3.1 as well. The calculated QYs are also given in Figure 3.5(d) (black dots). The measured and calculated QYs are in good agreement.

The decrease in photoluminescence decay lifetime and photoluminescence QY may indicate the presence of exciton migration in the NPL stacks due to Förster resonance energy transfer between the same type of NPLs, known as homo-NRET. Previously, it was shown that the exciton transfer within solids of the same quantum dot population decreases photoluminescence QY due to nonemissive QDs in the ensemble [58, 59]. Quenching in PL intensity was also observed in fluorescent dye solutions, accompanied by faster exciton decay, and similarly, the resulting changes in the exciton decay rate and PL intensity was attributed to quenching due to nonemissive dye dimers [60]. The theoretical model of Loring, Anderson and Fayer shows that such systems are prone to quenching due to trapping [61]. An exciton generated in a NPL of a stack is also expected to hop back and forth between NPLs due to strong dipole-dipole coupling between the face-to-face oriented NPLs. Since the NPLs are ordered in column-like assemblies, a generated exciton effectively makes a one-dimensional random walk between the NPLs of the same stack until it recombines. It was shown that when there is a trap in

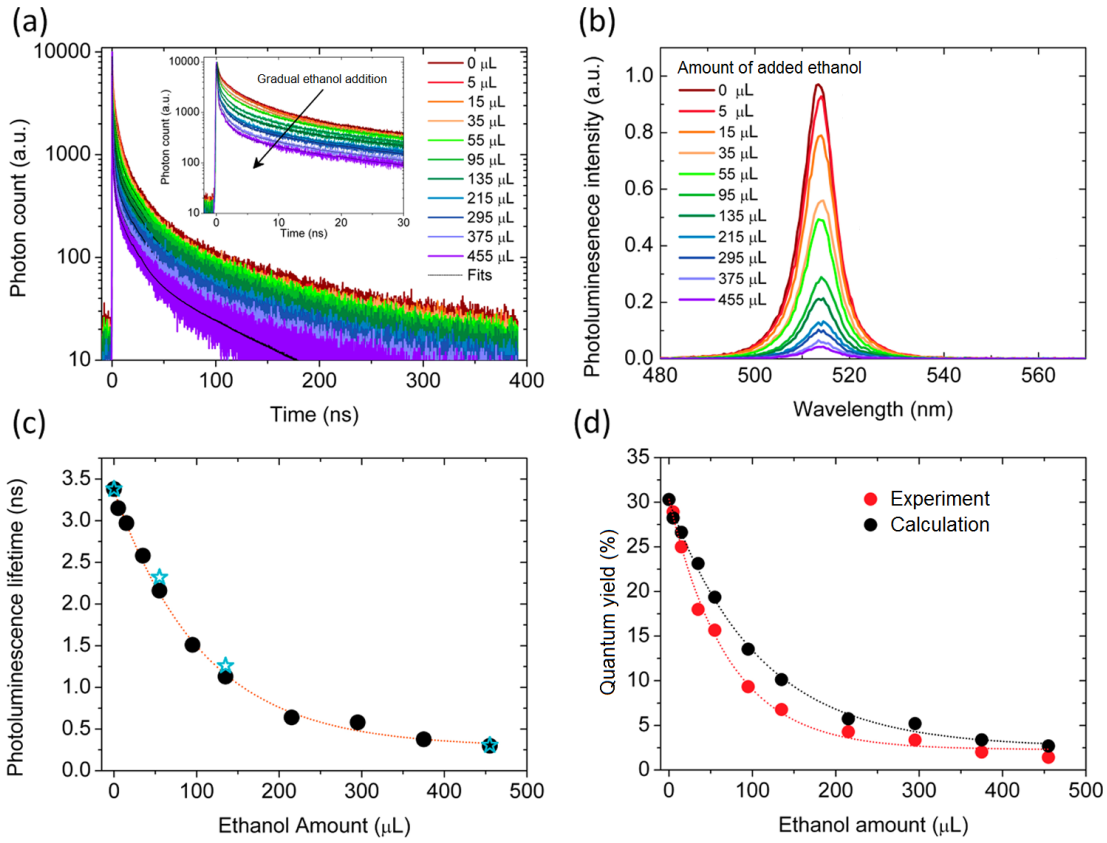

Figure 3.5: (a) Time-resolved photoluminescence decays together with their multiexponential fits. Inset shows the same photoluminescence decay curves in a shorter time window. (b) Steady-state photoluminescence intensity of the NPLs while ethanol is added gradually to the solution of the NPLs. (c) Amplitude-averaged photoluminescence lifetimes of the NPLs denoted by black dots as a function of the total added ethanol amount. Blue stars show the modeled photoluminescence lifetimes of the NPLs for 0, 55, 135, and 455 µL of ethanol added. (d) Photoluminescence QY of the NPLs as a function of the total added ethanol amount measured directly from steady-state photoluminescence measurements and calculated semiempirically from the photoluminescence lifetimes assuming the radiative recombination does not change. Reprinted by permission from [32] with copyright permission from ACS.

some of the excitation sites, the excitation decays get faster and the excitations are more likely to get trapped with the increasing number of trap sites [62].

Small Stokes shift enables a huge overlap between the absorbance and emission spectra of the NPLs, resulting in a large NRET rate between the NPLs. This rate has been approximated by calculating the Förster radius, the seperation distance between a donor and acceptor pair, at which the NRET efficiency is 50%, given by Eq. 2.2. In the calculation of R_0, the κ^2 term is taken as 4, which is its maximum value [51], because the transition dipoles are expected to be parallel and collinear. The other parameters used to predict the Förster radius are the QY of completely nonstacked NPLs, taken as 0.3, the refractive index n = 1.8; and the extinction coefficient of 3.1×10^{-14} cm^2 at 400 nm for 4 ML NPLs [38]. Finally, the center-to-center distance between neighbouring NPLs in a stack was measured as 4.29 nm using high-resolution TEM imaging. The NRET lifetime was then calculated to be ∼3 ps so that the NRET efficiency can be as high as 99.9%. The NRET between the neighboring NPLs in the same stack is thus much faster than the exciton recombination and excitons generated in a stack can hop back and forth within the NPL chain many times before eventually recombining.

3.2 Rate equations model

To explain the photoluminescence decay kinetics of the stacked NPLs, we developed a rate equation model that accounts for the NRET among the NPLs as well as the radiative and nonradiative recombination in these NPLs, along with an additional fast nonradiative recombination (i.e., hole trapping) in the NPLs having trap sites, referred to as the defected NPLs. We start by first considering a single type of NPL stack with a chain size k, in which the defected NPLs are located at certain NPL positions d_1, d_2..., d_m. Here, m denotes the number of the defected NPLs in the stack s, and $m \leq k$. For a set of the identical stacks, each with size k and trap sites located at the positions d_1, d_2..., d_m, we can construct the rate equations as follows:

$$
\begin{aligned}
\frac{dn_1}{dt} &= -(\gamma_1 + \gamma_{NRET})n_1 + \gamma_{NRET}n_2 \\
\frac{dn_2}{dt} &= -(\gamma_2 + 2\gamma_{NRET})n_2 + \gamma_{NRET}(n_1 + n_3) \\
&\vdots \\
\frac{dn_{k-1}}{dt} &= -(\gamma_{k-1} + 2\gamma_{NRET})n_{k-1} + \gamma_{NRET}(n_{k-2} + n_k) \\
\frac{dn_k}{dt} &= -(\gamma_k + \gamma_{NRET})n_k + \gamma_{NRET}n_{k-1}
\end{aligned}
\tag{3.2}
$$

Here, n_i denotes the number of excitons in the i$^{\text{th}}$ NPL of all the stacks in the set where i can be any integer from 1 to k. γ_{NRET} is the rate of exciton transfer between consecutive NPLs in a stack. γ_i is the recombination rate of each NPL and is defined as

$$
\gamma_i = \begin{cases} \gamma_{total} + \gamma_{trap}, & i = d_1, d_2 ... \text{ or } d_m \\ \gamma_{total}, & \text{otherwise} \end{cases}
\tag{3.3}
$$

where γ_{trap} is the charge trapping rate in the defected NPLs and $\gamma_{total} = \gamma_r + \gamma_{nr}$ is the sum of radiative and nonradiative recombination rates intrinsic to the nondefected NPLs. These rate equations can be put in the matrix form as

$$
\frac{d\bar{n}}{dt} = C\bar{n}
\tag{3.4}
$$

where $\bar{n} = \begin{bmatrix} n_1 \\ n_2 \\ \vdots \\ n_k \end{bmatrix}$ and

$$C = \begin{bmatrix} -(\gamma_1 + \gamma_{trap}) & \gamma_{trap} & 0 & \cdots & 0 \\ \gamma_{trap} & -(\gamma_2 + 2\gamma_{trap}) & \gamma_{trap} & \ddots & \vdots \\ 0 & \ddots & \ddots & \ddots & 0 \\ \vdots & \ddots & \gamma_{trap} & -(\gamma_{k-1} + 2\gamma_{trap}) & \gamma_{trap} \\ 0 & \cdots & 0 & \gamma_{trap} & -(\gamma_k + \gamma_{trap}) \end{bmatrix}$$

is the k-by-k coefficient matrix. The analytical solution can be found by taking the Laplace transform of both sides:

$$s\bar{N}(s) - \bar{n}(0) = C\bar{N}(s) \tag{3.5}$$

leading to

$$\bar{N}(s) = (s - IC)^{-1}\bar{n}(0) \tag{3.6}$$

Therefore, the analytical solution in the time domain is

$$\bar{n}(t) = \mathscr{L}^{-1}\{(s - IC)^{-1}\bar{n}(0)\} \tag{3.7}$$

where $\mathscr{L}^{-1}$ denotes the inverse Laplace transform operation.

Calculating the analytical solution can be cumbersome since there are stacks as long as 40 NPLs, as can be seen in Figure 3.3(c), or even longer. Therefore, the master equation was solved numerically to find $n(t)$ and to calculate the total exciton decay $s(t) = \sum_{i=1}^{k} n_i(t)$ for the subset of stacks in question. We used MATLAB's 'ode23' function to solve the numerical differential equations in the time invertal $0 \leq$ t ≤ 40 ns with a fixed time step of 4 ps.

Solving the master equation for some hypothetical stacks having several defected NPLs yields that $s(t)$ can be well fit with exponential decays. This can be seen in Figure 3.6, in which the solution of the rate equations is plotted for 3 different stacks. Exponential nature of the solution is expected because the rate $d\bar{n}/dt$ is proportional to $n(t)$. $s(t)$ can fit well to two exponentials in all three cases. Therefore, the solution is in the form of $s(t) = \sum_i A_i e^{-t/\tau_i}$, where A_i and τ_i are the amplitude and lifetime of the i$^{\text{th}}$ exponential component in the decay, respectively. Amplitude-averaged lifetime of the decay is given by

$$\tau_{stack} = \frac{\sum A_i \tau_i}{\sum A_i} \tag{3.8}$$

The quantities in the numerator and denominator can be readily calculated since $\sum A_i\tau_i$ is simply the area under the solution curve, i.e.,

$$\sum A_i\tau_i = \int_0^\infty s(t)dt \tag{3.9}$$

and similarly, the sum of amplitudes of all exponential components is simply the value of the solution at the first time instant:

$$\sum A_i = s(0) \tag{3.10}$$

yielding

$$\tau_{stack} = \frac{\int_0^\infty s(t)dt}{s(0)} \tag{3.11}$$

It is obvious that not only the number of defected NPLs in a stack, but also their positions affect the resulting photoluminescence lifetime of the NPL stack. To see the effect of the defected NPL location, we test the model on another hypothetical stack with 35 NPLs, only one of them being defected. The average PL lifetime of the stack as a function of the position of the defect is plotted in Figure 3.7. As can be seen in the figure, when the defect is closer to the side, the lifetime is longer. This can be explained by considering that, when the defected NPL is closer to the middle, it is more likely for an exciton to end up at the defect. When the defected NPL is on one side, however, the excitons on the other side should hop more times to reach the defect. It is more likely in the meantime for them to radiatively recombine in one of the nondefected NPLs. Hence, the average lifetime increases when the defect is closer to the side. The analysis can be extended to include multiple defects in a stack. However, in that case, all the defects should be located near one edge of the stack for lifetime elongation, which is not very likely in any case.

To calculate the average lifetime for a stacked NPL ensemble consisting of many stacks, we solve the master equation for different stacks and add up all of the $\sum A_i\tau_i$ terms coming from each solution on the numerator and $\sum A_i$ terms on the denominator to find the average lifetime for the whole ensemble. The sizes of the NPL stacks are determined according to the size distributions given in Figure 3.3. The final parameter to determine is the fraction of defected NPLs

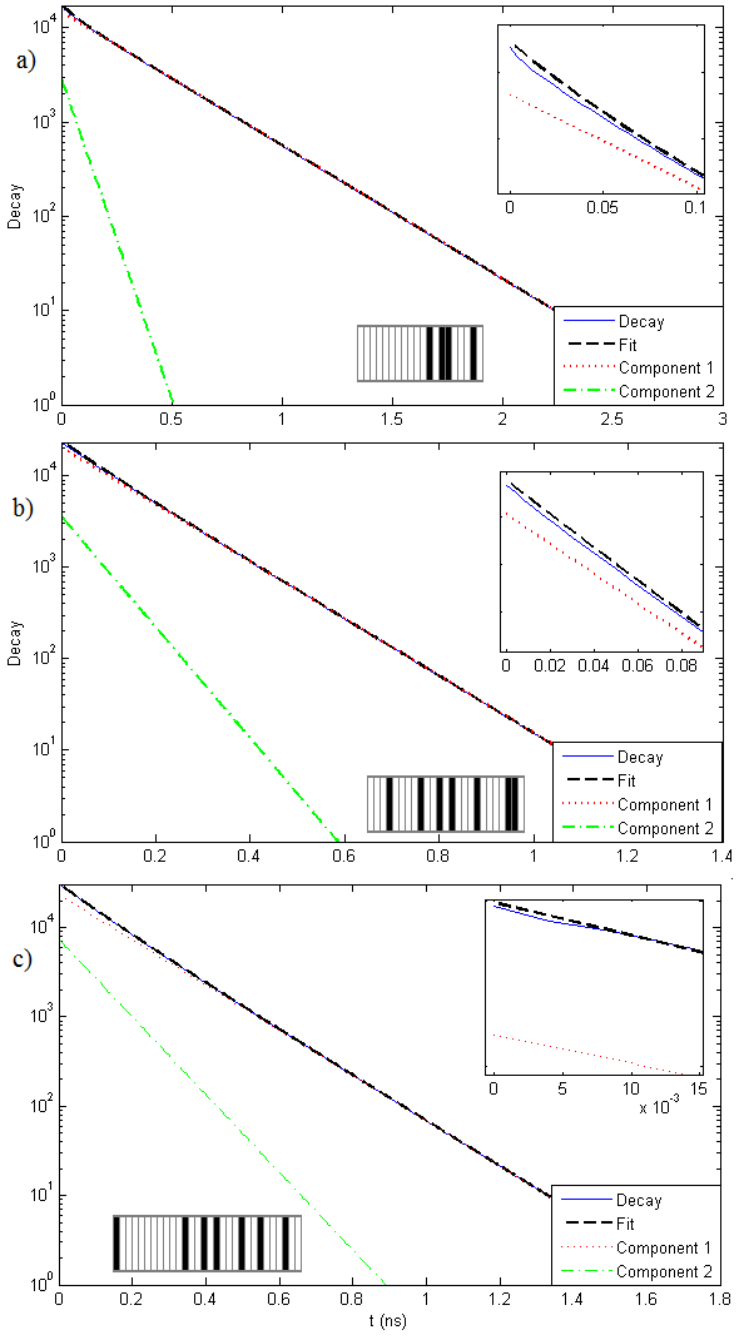

Figure 3.6: Multiexponential fittings for numerical solutions of the rate equations for the exemplary NPL stacks of size (a) 20, (b) 25 and (c) 30 with some of the NPLs defected. Insets show the same decays zoomed in the beginning of the curves. The NPL stacks for which the rate equations are solved are schematically illustrated at the bottom of each figure. Dark spots indicate the location of defected NPLs. The solid lines are the solution curves and the dashed lines are their fits. Plots are semi-logarithmic. Reprinted from Supplementary Information of [32].

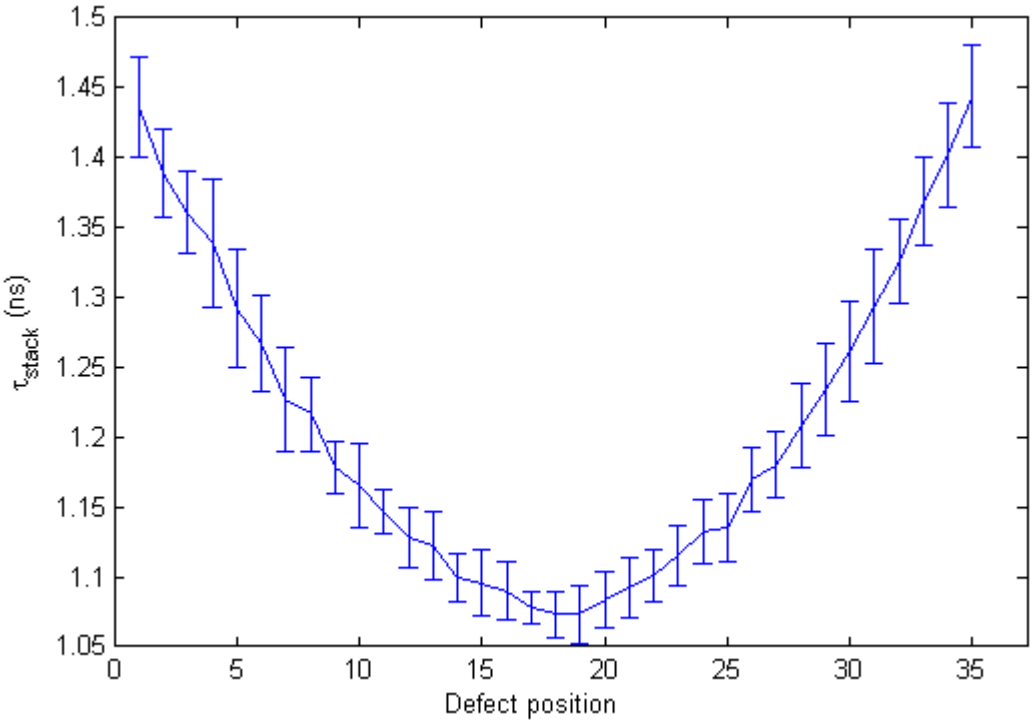

Figure 3.7: Computed average photoluminescence lifetime of a NPL stack depending on the position of the only defect in the stack. The stack has 35 NPLs. The lifetime parameters are τ_{total} = 3.38 ns, τ_{NRET} = 3 ps and τ_{trap} = 35 ps. Reprinted from the Supplementary Information of [32].

in the ensemble, namely r. Depending on the synthesis route or the lateral size of the NPLs, the resulting NPL populations may include different fractions of NPLs having trap sites [34]. It has also been verified by transient absorption measurements that some of the NPLs in the ensemble have trap sites [33]. To find r, we swept this parameter to match the estimated lifetime with the experimental lifetime of the ensemble with 55 µL of ethanol. We found that, when r = 0.22, the calculated decay time matches to the experimental lifetime. We use the same r for the other two cases of 135 and 455 µL ethanol, which we used to test the model. We calculated the PL lifetimes of the stacked NPLs in 55, 135, and 455 µL of ethanol added cases as 2.32, 1.26 and 0.31 ns, respectively. The calculated lifetimes are shown with blue stars in Figure 3.5(c). They display an excellent match with the experimental values of 2.16, 1.13 and 0.30 ns. This provides a vigorous support for the hypothesis that charge trapping assisted by homo-NRET is the dominant effect in changing the excitonic behaviour in these NPL stacks. Moreover, the fraction r = 0.22 works well with all three cases with different degrees of stacking, which elucidates that addition of ethanol does not create additional charge trapping sites.

3.3 Conclusion

In summary, it is demonstrated here that the stacked NPLs exhibit different transient and steady-state excitonic properties compared to the nonstacked NPLs. By controlling the degree of stacking gradually via addition of ethanol to the NPL dispersion, we observed that the PL emission intensity and the exciton decay times also gradually decrease. These observations are explained well by ultraefficient homo-NRET within the neighboring NPLs in a stack. Homo-NRET increases exciton trapping by causing excitons created in nondefected NPLs to end up in the defected ones. This results in strong quenching of the PL intensity and the acceleration of the decay rates beyond the level dictated by the fraction of the defected NPLs. We developed a rate equation based model to test our hypothesis. Constructing rate equations for a NPL stack with definite sizes and trap sites and then solving the rate equations for stacks of different sizes to find the general decay

curve and their decay times reveal that the lifetimes calculated by the model are in good agreement with the experimental measurements. The results of this study indicate that the change in the transient and steady-state emission properties of the NPL stacks can be attributed to increased homo-NRET.

Chapter 4

Temperature-dependent time-resolved optical spectroscopy study and quantum yield estimations of stacked nanoplatelets using Markov chains

Our second approach to develop a deeper understanding of the effect of stacking on exciton dynamics in colloidal nanoplatelets is to make use of Markov chains to model the excitonic transitions in NPL stacks. By calculating the recombination, energy transfer, and hole trapping probabilities associated with excitons in NPL stacks, we estimated the average photoluminescence lifetime and quantum yield for stacked NPL ensembles. This model was used in our study in which the transient and steady-state photoluminescence kinetics of 4 ML CdSe nanoplatelets is comparatively investigated at different temperatures for nonstacked and stacked solid film ensembles. To this end, temperature-dependent PL intensity spectra

and transient decays of the NPL ensembles were investigated and analyzed. It has been found out that there are important differences between the nonstacked and stacked NPLs in terms of excitonic properties. While the nonstacked NPLs display a notable increase in their PL emission intensity at lower temperatures, this increase is quite limited in stacked NPLs. Moreover, the photoluminescence lifetimes of stacked NPLs are much shorter than those of the nonstacked ones at all temperatures.

In order to account for these differences, we use the fact that there is very fast Förster resonance energy transfer (FRET) between the NPLs in a stack, as we did in our previous work [32]. Here we develop another model to explain the differences in excitonic properties of nonstacked and stacked NPLs. The excitonic transitions in a stack are modeled as a Markov chain, and we estimate the likelihood of radiative recombination of an exciton in the stack, as well as how long an exciton can endure without decaying via traps in the charge trapping sites. Our simulation results are in good agreement with the experimental data, and we show that the competition between the radiative recombination rate and hole trapping, both of which increase with decreasing temperature, causes a weakly temperature-sensitive behaviour in stacked NPLs in terms of steady-state PL, compared to nonstacked NPLs.

This chapter is partially taken from one of the recent journal publication articles of our group, which is in the submission process. The author of this thesis is the first author on that study.

4.1 Experiment

4.1.1 Sample preparation

A recipe modified from Ref. [15] was used to synthesize 4 ML CdSe NPLs. 340 mg of cadmium myristate, 24 mg of selenium powder and 30 mL of octadecene were loaded into a three-neck flask of 100 mL volume. The mixed solution was

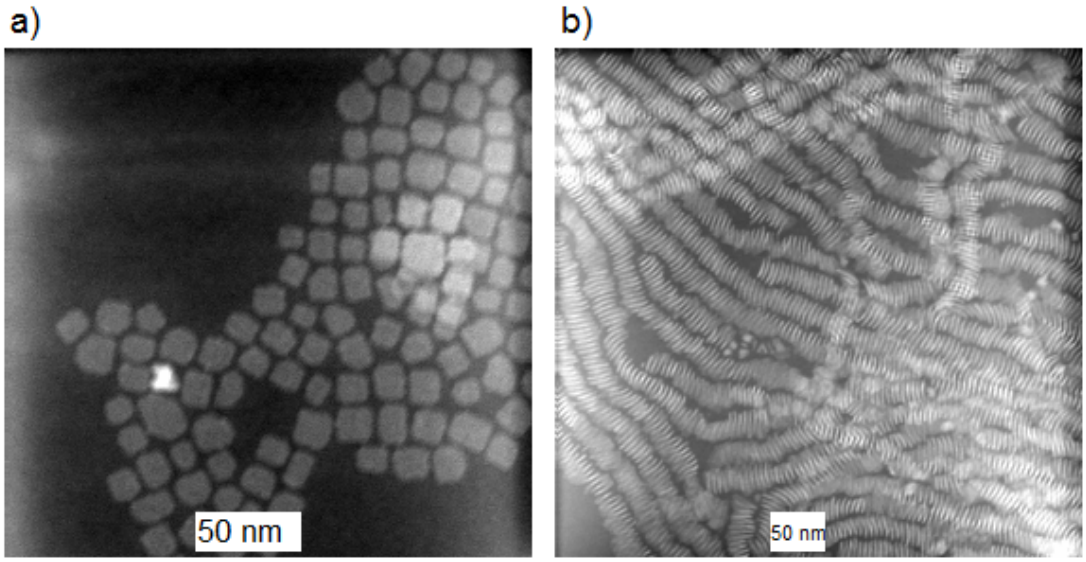

Figure 4.1: HAADF-TEM imaging of (a) non-stacked and (b) stacked NPL ensembles.

kept under vacuum for 1 h at room temperature. Then, the solution was heated to 240 °C under argon atmosphere. At 195 °C, 120 mg of cadmium acetate dihydrate was quickly added into the flask. The NPLs were grown at 240 °C for 10 min and the system was cooled down to room temperature. A setup similar to the one in Figure 3.1 was used for the synthesis.

After the cooldown is complete, 1 mL of oleic acid was added to the solution. The overall solution was dissolved in hexane. The mixture was centrifuged at 14,500 rpm for 10 min and the supernatant part was removed from the centrifuge tube. The precipitate was dissolved in hexane again and centrifuged at 4,500 rpm for 5 min. This time, the supernatant part was separated into another centrifuge tube and ethanol was added into the solution until it became turbid. The solution was once again centrifigued at 4,500 rpm for 5 min and the resulting precipitate was dissolved in hexane. Finally, the solution was filtered using a 0.20 µm particle filter. The HAADF-TEM imaging of the NPLs are shown in Figure 4.1. In the stacked ensemble, all the observed NPLs are in stacked formation.

The NPLs were immobilized on 1.2 cm x 1.2 cm quartz substrates. To make non-stacked NPL films, the NPL solution was spin-coated. To make stacked NPL

ensemble, the solution was drop-cast onto the substrate. The films were used for both the TRF and steady-state PL measurements.

4.1.2 Experimental setup

We studied the time-resolved fluorescence (TRF) decays and steady-state photoluminescence (PL) spectra of stacked and nonstacked ensembles at different temperatures. A modifed version of the setup in Figure 3.4 was used to take temperature-dependent TRF and PL measurements under vacuum. The complete setup is shown in Figure 4.2. The NPL film on substrate is placed onto the sample holder shown in Figure 4.2(a). The sample holder is inside a cryostat. The part of the cryostat with the sample holder is placed inside the sample chamber. There are windows in this part of the cryostat to allow the excitation pump in, as well as to let out the emission from the sample. The emitted light is collected both by the photomultiplier tube (PMT) and by a spectrometer (Maya 2000) with the help of a fiber-optic cable, as seen in Figure 4.2(b). The light that scatters towards the PMT side is used for time-resolved photoluminescence decay measurements. The light that scatters towards the fiber-optic cable is used for steady-state photoluminescence (PL) measurements. The fiber-optic cable is fixed such that its edge hovers right over the cryostat in order to achieve good coupling between the cable and the emitted light.

To adjust the temperature of the samples, we used a closed cycle helium cryostat together with a temperature-controlled heater. After the cryostat was taken into vacuum with the help of a vacuum pump, helium with temperature around 5 K was continuously pumped to decrease the temperature. In order to fix the temperature at a particular value, we used a heater and its feedback controller to introduce heat and stabilize the temperature around the sample holder. Our system is capable of reducing the temperature of the sample down to 20 K.

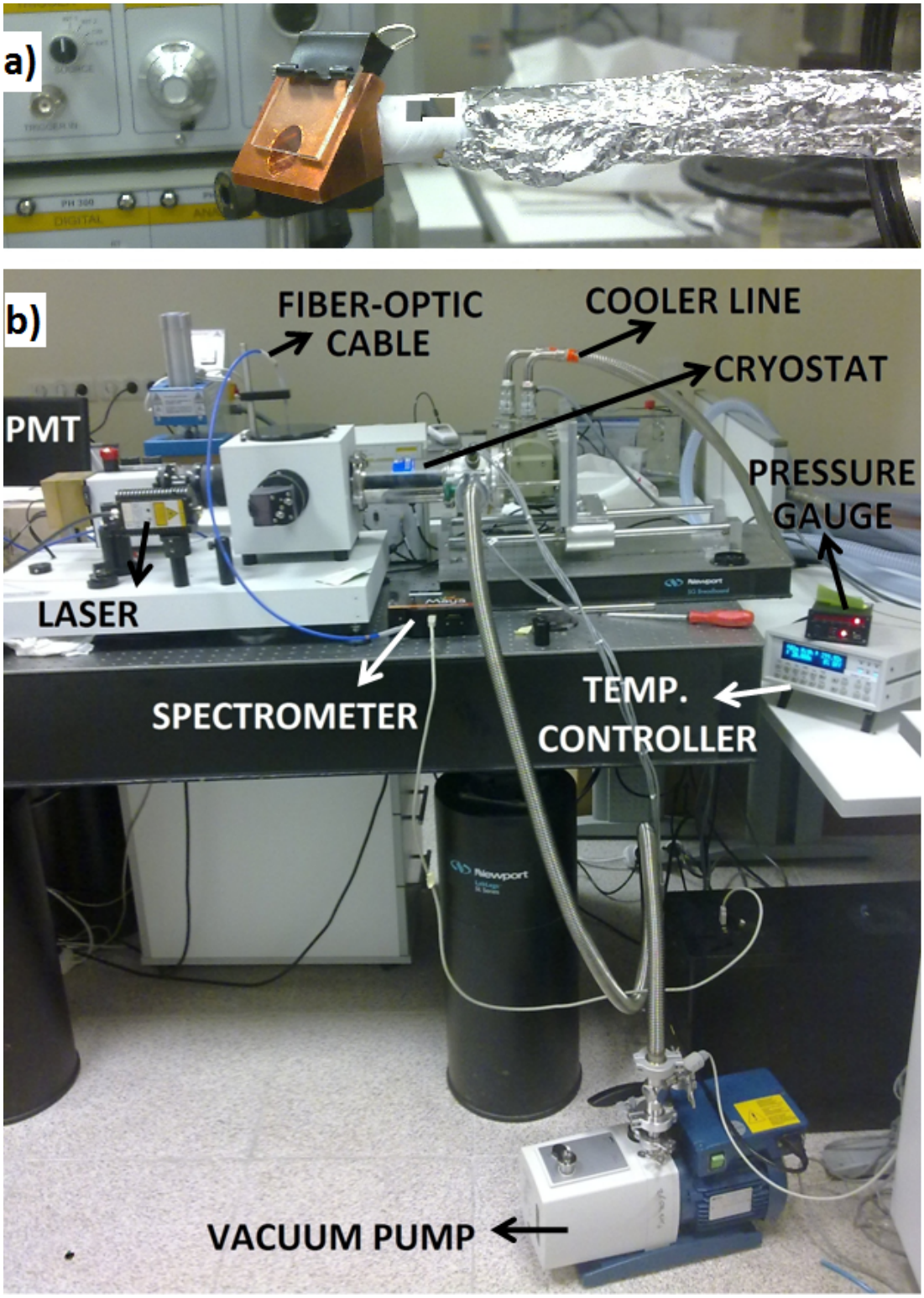

Figure 4.2: Experimental setup for the temperature-dependent TRF and steady-state PL measurements. (a) 2 cm by 2 cm sample holder inside the cryostat and (b) complete setup for temperature-dependent TRF and PL measurements in vacuum at our Bilkent UNAM laboratory.

4.1.3 Results and discussion

The TRF and steady-state PL measurements were carried out at certain temperatures ranging from room temperature (RT@297 K) down to 150 K. The results for both the stacked and nonstacked ensembles are summarized in Figure 4.3. Figures 4.3(a) and 4.3(b) display the PL spectra at different temperatures for the nonstacked and stacked ensembles, respectively. The PL emission peak of the nonstacked NPL ensemble is 2.41 eV (∼514 nm) at RT and blue-shifts to 2.45 eV (∼506 nm) at 150 K. The FWHM of the PL spectrum is 41 meV (8.8 nm) at room temperature. With decreasing temperature, the FWHM gets narrower. At 150 K, the FWHM is 25 meV (5.1 nm). For the stacked ensemble, the PL emission peak is 2.40 eV at RT and 2.44 eV at 150 K, while the FWHM narrows down from 47.3 meV at RT to 35.1 meV at 150 K. The slightly red-shifted PL with a wider FWHM in the stacked ensemble could be attributed to increased dielectric constant of the environment seen by the NPLs due to their dense packing when stacked.

The measurements reveal that the bandgap emission of the nonstacked ensemble increases by 1.4 folds when the temperature is reduced from RT to 150 K, whereas the increase in the stacked ensemble is only 1.08 folds. The time-resolved emission intensity decays of the nonstacked and stacked ensembles as a function of temperature are shown in Figures 4.3(d) and 4.3(e), respectively. The amplitude-averaged lifetimes (τ_{avg}) at each temperature are given in Figure 4.3(f), for both nonstacked and stacked ensembles. In both cases, the lifetimes get shorter with decreasing temperature. For the nonstacked ensemble, the lifetime at room temperature was measured to be 1.8 ns and it reduced to 0.58 ns at 150 K. On the other hand, the RT lifetime of the stacked ensemble was only 0.27 ns and reduced to 47 ps at 150 K.

It can be seen that there are stark differences between the nonstacked and stacked NPL ensembles in terms of both transient and steady-state PL behaviour. From RT down to 150 K, the PL intensity increases by 40% in the nonstacked ensemble, similar to a previous report on CdSe NPLs [16]. In the stacked ensemble, however,

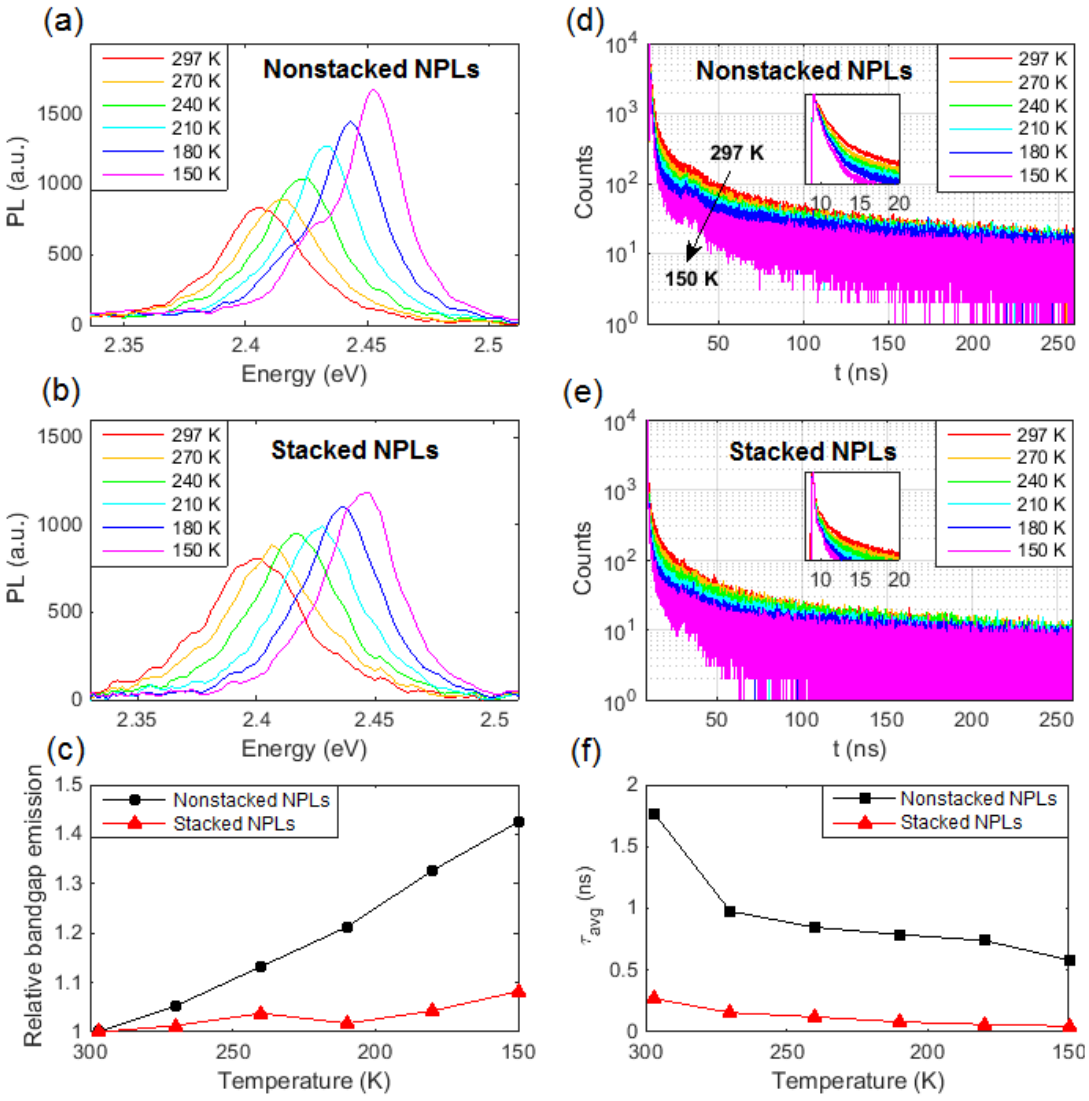

Figure 4.3: PL intensity spectra of (a) nonstacked and (b) stacked NPL ensembles at different temperatures. (c) Change in PL intensity of nonstacked (black square) and stacked (red triangle) NPL ensembles, relative to their PL intensities at room temperature. Transient photoluminescence decays of (d) the nonstacked and (e) stacked ensembles. Insets show the same decay curves in a shorter time window. (f) Fluorescence lifetimes of the nonstacked (black square) and stacked (red triangle) NPL ensembles as a function of temperature.

the PL intensity is almost constant with temperature. The increase in the PL intensity at 150 K is only 8%. Moreover, the lifetimes in the stacked ensemble are much shorter than the lifetimes in the nonstacked one. This is in agreement with our previous report, where we demonstrated that the PL decays are much faster in stacked ensembles [32]. In that work, we showed that fast exciton transfer between the NPLs in a stack resulted in the excitons ending up in charge traps that exist only in a minor subpopulation of the NPLs, which reduces both the QY and PL decay lifetime of stacked NPL ensembles [32].

In order to explain the differences between the stacked and nonstacked ensembles in terms of temperature-dependent excitonic dynamics, we used a similar approach here. We consider homo-FRET, which is known to take place at a very fast rate between neighboring NPLs in a stack [31, 32], along with occasional charge trapping in NPLs [33, 63]. It was shown that a NPL population can have a significant amount of NPLs with a trap site [33]. These sites may trap charges at a high rate, resulting in very low QYs in the NPLs having these trap sites. With high FRET efficiency within a stack, excitons are expected to hop back and forth in the NPLs of a stack before they recombine [32]. Therefore, an exciton, which is initially generated upon the absorption of a photon by a single NPL containing no trap site (i.e., defect), may actually end up in a defect of another NPL. This is expected to reduce both the QY and the exciton decay lifetimes.

Previously, dynamics of electronic excitations in single- and multi-dimensional arrays have been studied for a wide range of materials including QDs [59] and concentrated dye solutions [60]. In both studies, quenching in photoluminescence is observed, and it was also shown that the reason for the quenching is the energy transfer between the donors. Similar systems in which excitation energy can travel in a lattice of excitation sites with some having traps, have been analytically studied. Kulak and Bojarski developed a model for a system with acceptors that can transfer energy back to the donors so that two-way excitation transfer is possible between the donor and acceptor [64, 65]. Montroll's work on photosynthetic units with one particular site to collect the excitation, which can make random walk on chlorophyll units, estimates the mean lifetime of an excitation until it ends up in the collection site [66]. The decay of the excitation

in one-dimensional (1D) lattices in the presence of traps have been parametrically studied by Sanchez et al. [62]. These studies show that even when a small fraction of the excitation nodes are traps, a considerable amount of the excitations end up being trapped, and the excitation decays get dramatically faster.

The situation in the NPL stacks is similar to the systems discussed above. Excitons are expected to pass through the traps during their 1D random walk throughout the NPL stacks. The defected NPLs are not perfect trap sites, i.e., they do not trap all the excitons that visit them but instead introduce a certain probability of charge trapping, depending on the finite trapping rate. As a result, an exciton in a defected NPL may get trapped, but also it can still undergo radiative recombination or FRET. Our model investigates how the existence of such traps affects the transient photoluminescence as well as the quantum yield.

4.2 Model and simulations

We start by considering an exciton in a NPL stack. At a time instant, the exciton can reside at any of the NPLs. Within an infinitesimally short period of time, there is a probability that this exciton recombines, gets transferred to one of its neighbouring NPLs, or stays in the same NPL. It can be realized that the probability of the exciton being in a particular NPL in the stack is determined merely by its previous location. The system can therefore be regarded as a Markov chain. Figure 4.4(a) illustrates a stack in which some of the NPLs are defected. The discrete-time Markov chain that represents the excitonic transitions in this stack is depicted in Figure 4.4. The states of the system are shown by circles. At t = 0, the system is at state zero, corresopnding to prior to the absorption of a photon. Since each NPL in the stack is equally likely to absorb a photon, the probability of transition from state zero to any of the NPL states is $p_{0,i} = 1/k$, where $1 < i < k$ and k is the number of NPLs in the stack. The remaining two states, R and NR, account for radiative and nonradiative recombination, respectively. Once the system is in either R or NR state, it stays in that state thereafter, i.e., $p_{R,R} = p_{NR,NR} = 1$. The physical meaning is that once the system

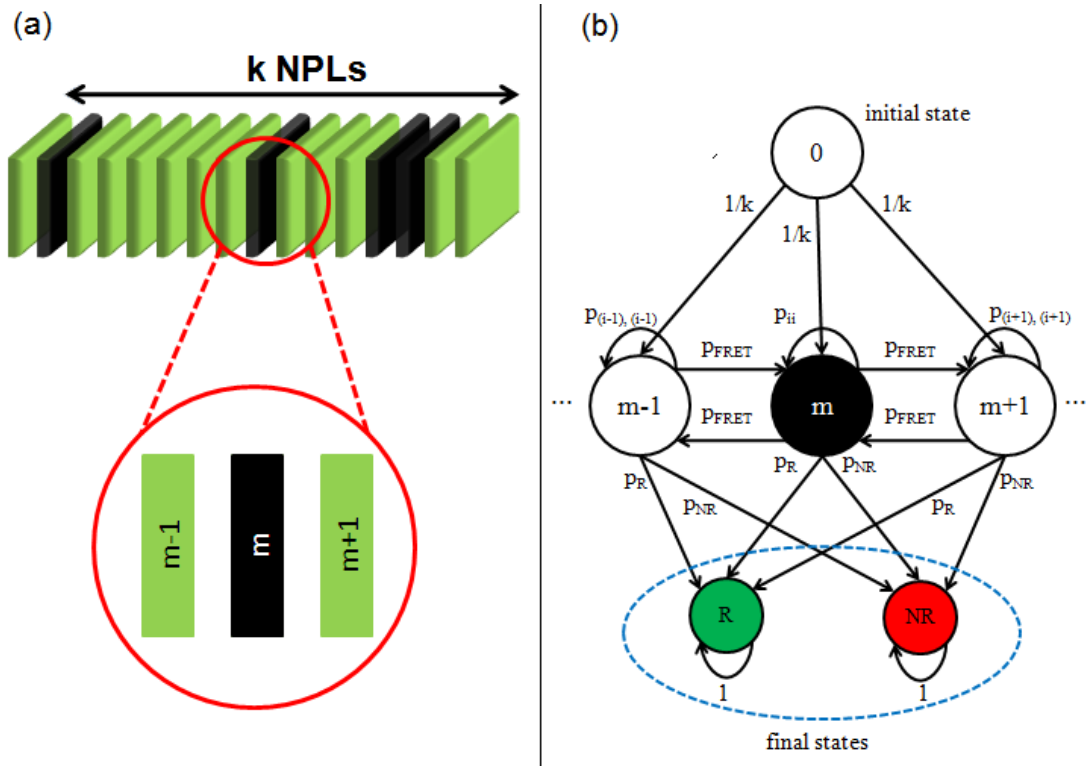

Figure 4.4: (a) Illustration of an exemplary NPL stack with some defect sites (shown in black). (b) Some of the states and transitions in the Markov chain used to model excitonic transitions in the stack drawn in (a). States m-1, m and m+1 correspond to the exciton being m-1'th, m'th or m+1'th stack, respectively. Other states from 1 to k, where k is the number of NPLs in the stack, are not drawn. The initial state is state 0, and the system will end up in R or NR state, which correspond to radiative and nonradiative recombination, respectively. Transition probabilities are determined by the transition rates.

is in R (NR), the exciton recombines radiatively (nonradiatively).

The PL lifetime and QY of a stack are determined by the number of defected NPLs in the stack, as well as their locations on the stack. The number of the defected NPLs in a stack is determined to a great extent by the proportion of the defected NPLs in the overall NPL ensemble. This proportion may depend on the synthesis methodology and the lateral size of the NPLs [33, 34]. The defects are expected be distributed randomly around the stack. If a randomly walking exciton ends up in any one of these defected NPLs, it becomes much more likely for that exciton to recombine nonradiatively due to the charge trap. We can calculate the expected survival duration of an exciton in a stack as well as the

probability of radiative recombination from any of the NPLs.

The transition probabilities in the Markov chain described above depend on the radiative and nonradiative recombination rates as well as FRET and charge trapping rates. Additionally, in order to work in a discrete time domain, we define a small time step Δt. In our calculations, we assume the following:

- More than one exciton does not exist simultaneously in a NPL stack.
- NPLs in a stack can transfer excitons only to a neighboring NPL and not to the NPLs further away.
- Defected NPLs do not contribute to the emission in nonstacked ensembles.
- The spacing between the NPLs in a stack is constant (4.29 nm) [32]. Moreover, the NPLs in a stack do not have variation in lateral size and they are in complete face-to-face orientation.
- Exciton transfer takes place only via nonradiative energy transfer and not the radiative one.

We then move on to construct the transition probability matrix P of the Markov chain that is used to model the transitions in an arbitrary stack s containing k NPLs as follows. If $\gamma_r(\gamma_{nr})$ is the radiative (nonradiative) exciton recombination rate in the NPLs, γ_{FRET} is the rate of FRET between the neighboring NPLs, and γ_{trap} is the rate of charge trapping at a defected NPL, then the probability of radiative recombination from any NPL in the stack is

$$p_{i,R} = \gamma_r \Delta t \tag{4.1}$$

where Δt is the time step, and the state i can be anything from 1 to k, and similarly

$$\gamma_{i,NR} = \begin{cases} \gamma_{nr}\Delta t, & \text{if i is not defected} \\ (\gamma_{nr} + \gamma_{trap})\Delta t, & \text{if i is defected} \end{cases} \tag{4.2}$$

The exciton transfer is only between the neighboring NPLs. Given our assumptions, the transfer rate is always the same (γ_{FRET}). We have

$$p_{i,(i+1)} = p_{j,(j-1)} = p_{FRET} = \gamma_{FRET}\Delta t \tag{4.3}$$

for i = 1, 2..., k-1, and j = 2, 3..., k

An exciton does not necessarily recombine or hop into another NPL within a time interval. The probability that the exciton stays in the same location, i.e., the state of the system does not change in between t and t + Δt, is

$$p_{i,i} = \begin{cases} 1 - (p_{i,R} + p_{i,NR} + p_{FRET}), & i = 1 \text{ or } i = k \\ 1 - (p_{i,R} + p_{i,NR} + 2p_{FRET}), & 1 < i < k \end{cases} \tag{4.4}$$

Finally, as stated above,

$$p_{R,R} = p_{NR,NR} = 1 \tag{4.5}$$

This completes the construction of the Markov chain since for any state in the Markov chain, the sum of transition probabilities to all states is unity.

4.2.1 Calculation of quantum yield and photoluminescence lifetime of stacked nanoplatelets

After all the transition probabilities are determined, the average PL lifetime and QY of the stack can be calculated. We are going to first derive the expression for

the QY of a stack as it is more straightforward. Let

$$P = \begin{bmatrix} p_{0,0} & p_{0,1} & p_{0,2} & \cdots & p_{0,k} & p_{0,R} & p_{0,NR} \\ p_{1,0} & p_{1,1} & p_{1,2} & \cdots & p_{1,k} & p_{1,R} & p_{1,NR} \\ p_{2,0} & p_{2,1} & p_{2,2} & \cdots & p_{2,k} & p_{2,R} & p_{2,NR} \\ \vdots & \vdots & \vdots & \ddots & \vdots & \vdots & \vdots \\ p_{k,0} & p_{k,1} & p_{k,2} & \cdots & p_{k,k} & p_{k,R} & p_{k,NR} \\ p_{R,0} & p_{R,1} & p_{R,2} & \cdots & p_{R,k} & p_{R,R} & p_{R,NR} \\ p_{NR,0} & p_{NR,1} & p_{NR,2} & \cdots & p_{NR,k} & p_{NR,R} & p_{NR,NR} \end{bmatrix}$$

be the (k+3)-by-(k+3) transition probability matrix for an artibrary stack of k NPLs. By calculating powers of P, we can find out the probability that the state is R after a particular number of steps, as well as the probability of "arrival" at state R after a certain number of steps. The QY of a stack is simply the probability that the system eventually arrives at state R. To find out how this can be calculated, we first focus on how the radiative recombination at a particular time instant can be found.

As can be seen in Figure 4.4(b), the fastest radiative recombination can take place in two steps. The probability that the system is at state R after the second step is given by $(P^2)_{0,R}$. This is also equal to the probability of "arrival" at state R at the second step. $(P^n)_{0,R}$ for n >2, however, is not equal to the probability of arrival at R at the n^{th} step. $(P^n)_{0,R}$ includes the cases in which the first arrival at R is in the n^{th} step as well as earlier arrivals at R followed by successive R to R transitions. That is,

$$(P^n)_{0,R} = (P^{n-1})_{0,R} \times P_{R,R} + \sum_{i=1}^{k} \left((P^{n-1})_{0,i} \times P_{i,R} \right) \tag{4.6}$$

In this expression, the first term corresponds to the cases in which the system arrives at the R state before the n^{th} step, and simply makes an R→R transition in the final (n^{th}) step. The second term corresponds to the cases in which the first transition to R takes place at the n^{th} step. This term therefore yields the probability that a photon is emitted at the n^{th} step. Defining the probability p_n

of photon emission at the n$^{\text{th}}$ step as

$$p_n = \sum_{i=1}^{k} \left((P^{n-1})_{0,i} \times P_{i,R} \right) \tag{4.7}$$

we see that

$$p_n = (P^n)_{0,R} - (P^{n-1})_{0,R} \times P_{R,R} \tag{4.8}$$

but $P_{R,R} = 1$, so

$$p_n = (P^n)_{0,R} - (P^{n-1})_{0,R} \tag{4.9}$$

We have therefore shown that the probability of photon emission at any given time instant can be calculated using the transition probability matrix P. We can now calculate the QY as the probability that the exciton in the NPL stack recombines radiatively at any time, i.e.,

$$QY_{stack} = \sum_{i=1}^{\infty} p_i \tag{4.10}$$

Using Eq. 4.9, we can reexpress Eq. 4.10 as

$$QY_{stack} = \lim_{n \to \infty} (P^n)_{0,R} \tag{4.11}$$

To calculate the average PL lifetime of a stack, we make use of the p_n as a function of n. Like a TRF measurement in which photons detected in each bin are counted, calculation of p_n determines the probability of photon emission at different time bins. The analogy can be seen more easily when p_n is plotted as a function of n. This is done for three hypothetical NPL stacks in Figure 4.5. As can be seen in the figure, p_n decays exponentially with n. In general, this decay is multiexponential in the form $s(t) = \sum_j A_j e^{-t/\tau_j}$, where A_j and τ_j are the amplitude and lifetime of the j$^{\text{th}}$ decay component, respectively. Following a similar discussion as in Section 3.2, we obtain,

$$\tau_{stack} = \frac{\int_0^{\infty} s(t) dt}{s(0)} \tag{4.12}$$

The numerator is the area under the decay curve. For our discrete-time signal p_n, this area can be calculated simply by

$$\int_0^\infty s(t)dt = \Delta t \sum_{i=1}^{\infty} p_n = \lim_{n\to\infty} (P^n)_{0,R} \times \Delta t \tag{4.13}$$

The denominator is the sum of amplitudes of all the decay components, which is basically the probability of photon emission between t = 0 and t = Δt, i.e.,

$$s(0) = (P^2)_{0,R} \tag{4.14}$$

yielding the average lifetime to be

$$\tau_{stack} = \frac{\lim\limits_{n\to\infty} (P^n)_{0,R}}{(P^2)_{0,R}} \Delta t \tag{4.15}$$

An extension of this discussion can be used to calculate the overall PL lifetime and QY for a collection of non-identical NPL stacks in an ensemble, as we will do in Section 4.2.1.2.

4.2.1.1 Calculations for a single NPL stack

To calculate the PL lifetime and QY of a NPL stack, we directly use Eqs. 4.11 and 4.15. In Figure 4.5, we show the calculated QY and photoluminescence decays for three exemplary NPL stacks, with some of their NPLs defected. The parameters used for the calculations are the quantum yield of the nondefected NPLs (0.15), PL lifetime of nonstacked NPL ensembles (1 ns), hole trapping rate ($(10\ ps)^{-1}$) and FRET rate ($(25\ ps)^{-1}$). After the transition probability matrix P was constructed, we calculated the photoluminescence decay. The decay of p_n is presented for each case in Figure 4.5. As can be seen in the figure, all three decays are multiexponential, and they can be fit very well with two exponential

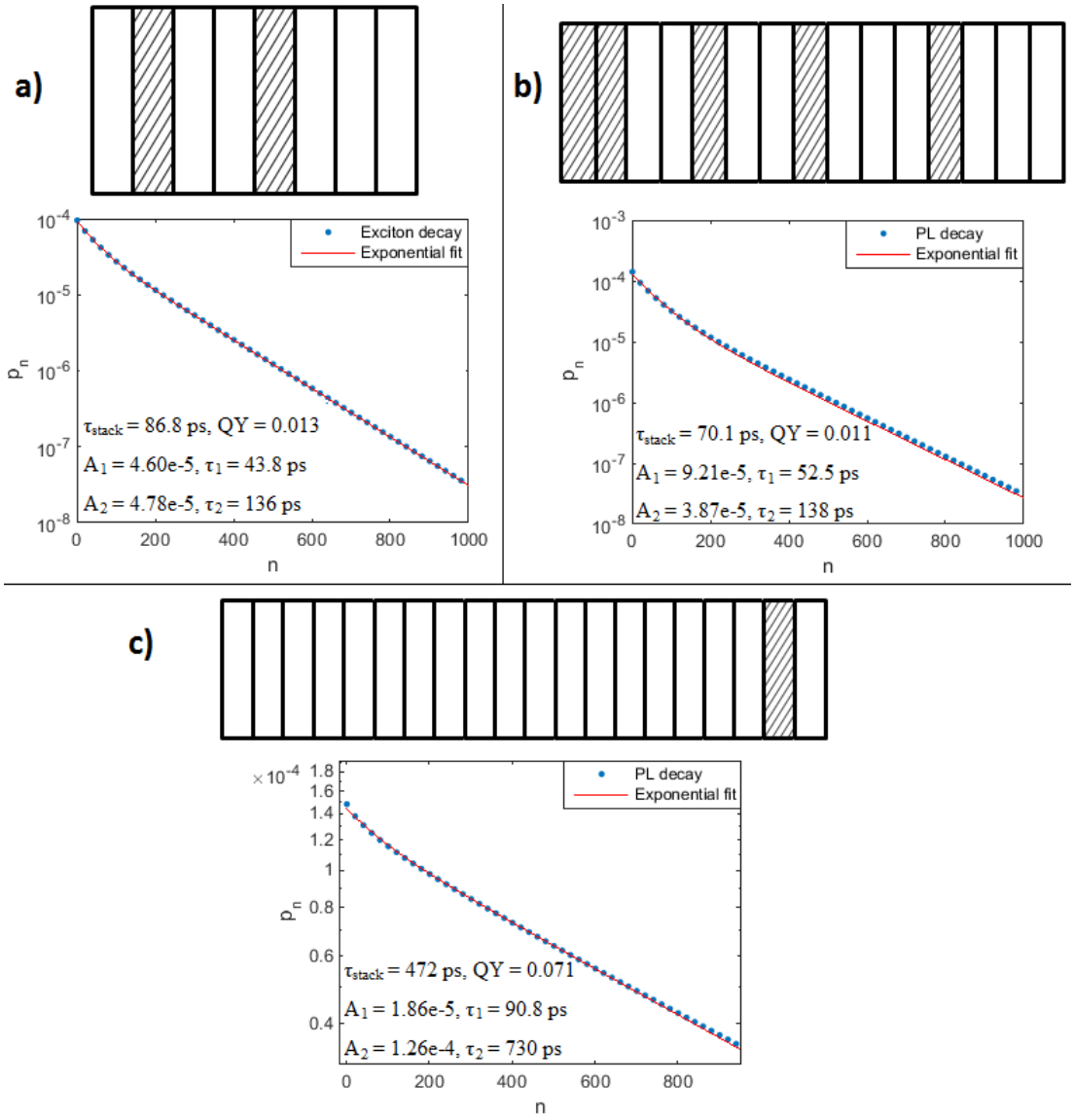

Figure 4.5: Time-resolved PL decays for hypothetical NPL stacks. The resulting QY, amplitude-averaged lifetime and the parameters of exponential terms used to fit the PL decay are given in the insets.

components. It was observed that the number of exponentials required for a good fitting of the PL decay may be three for some NPL stacks as well. The resulting average lifetimes and QYs are given inside the figures. We observe that, as more and more defects are introduced into a NPL stack, the PL lifetime tends to decrease, and so does the QY. The stack with the densest defect population is the one in Figure 4.5(b), and it has the lowest QY and PL lifetime. On the other hand, the NPL stack in Figure 4.5(c) has only one defected NPL out of 20 NPLs, and its PL lifetime and QY are very high compared to the other two cases.

4.2.1.2 Calculations for a stacked NPL ensemble

Next, we move on to calculate the QY and PL lifetime of an ensemble composed of many NPL stacks with different sizes. Since the transient PL signals of individual NPL stacks have been shown to be multiexponential decays, we can deduce that a PL signal coming from many NPL stacks is also a multiexponential decay with many different exponential components. We can still calculate the average PL lifetime and the QY in a similar manner. If the excited portion of a NPL ensemble is composed of stacks s_1, s_2... and s_N, where N is the number of NPL stacks that are excited by the pump, and the transition probability matrices for these NPL stacks are P_{s_1}, P_{s_2}... P_{s_N} respectively, the amplitude-averaged lifetime of the ensemble can be found by

$$\tau_{avg} = \frac{\sum_{i=1}^{N} \left(k_i \lim_{n\to\infty} (P_{s_i}^n)_{0,R} \right)}{\left(\sum_{i=1}^{N} k_i \right) \left(\sum_{i=1}^{N} (P_{s_i}^2)_{0,R} \right)} \Delta t \tag{4.16}$$

where k_i is the number of NPLs in the i$^{\text{th}}$ stack. The QY of the ensemble is

$$QY = \frac{\sum_{i=1}^{N} \left(k_i \lim_{n\to\infty} (P_{s_i}^n)_{0,R} \right)}{\sum_{i=1}^{N} k_i} \tag{4.17}$$

In the calculations for a stacked ensemble, we consider that a stack with more NPLs is longer and therefore will have a larger absorption cross-section, and is more likely to absorb a photon than the shorter ones. We assumed that the absorption cross section of a NPL stack is proportional to the number of NPLs in a stack. This assumption is justified as all the NPL stacks in the ensemble are standing perpendicular on the substrate as shown in Figure 4.1(b). As a result, the active area of a NPL stack seen by incident photons are approximately proportional to k_i Therefore, the contribution of NPL stacks to transient and steady-state emission is weighted by the number of NPLs they have.

4.2.1.2.1 Parameter study of the model for the lifetime and QY estimation of stacked NPL ensembles. We can now move on to estimate the temperature-dependent PL lifetime and QY of the stacked ensemble used in the experiments. To this end, we need to know QY of a nondefected NPL at a particular temperature, fraction of defected NPLs in the ensemble, radiative and nonradiative recombination rates intrinsic to the NPLs, FRET rate between the neighboring NPLs in a stack, trapping rate in defected NPLs, and size distribution of the NPL stacks in terms of the number of NPLs they have. To determine the exciton recombination and FRET rates, we use the experimental data of the nonstacked NPL ensemble. The QY of an emitter is given by

$$QY = \frac{\gamma_r}{\gamma_{total}} = \frac{\gamma_r}{\gamma_r + \gamma_{nr}} \tag{4.18}$$

$\gamma_{total} = 1/\tau_{total}$ is known from the TRF measurements and can be used to calculate γ_r and γ_{nr}. However, it was rendered practically impossible to make QY measurements of thin films and it was not possible for the integrating sphere to collect sufficient emission. Therefore, in the calculations, QY of the non-defected NPLs were set as a variational parameter. Using the temperature-dependent steady-state PL spectra of nonstacked NPLs, which are shown in Figure 4.6, we were able to set an upper bound on the value of QY at room temperature in vacuum. The complete emission spectrum includes two main features: One around 500 nm is the bandgap emission and the other one, which is much wider and

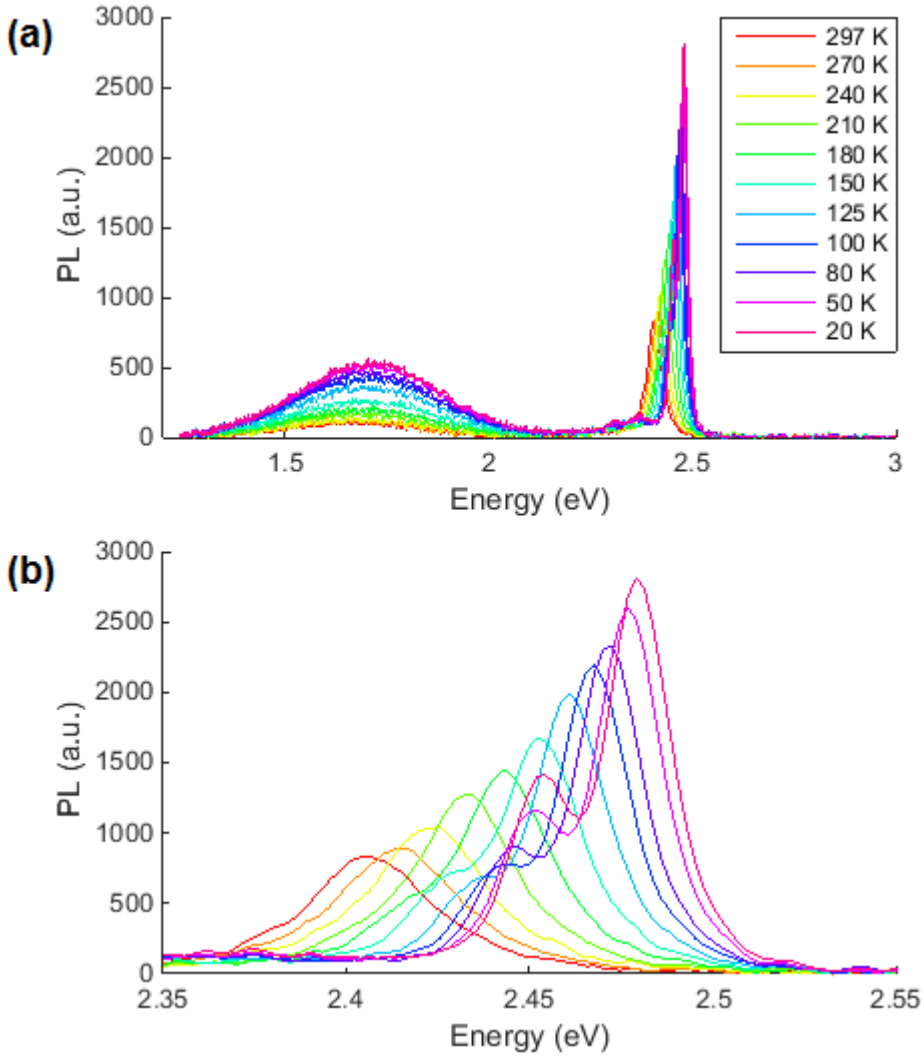

Figure 4.6: (a) PL spectra of the nonstacked NPLs at different temperatures, which include both the bandgap and trap emissions. (b) PL spectra focusing on the bandgap emission.

Table 4.1: Lorentzian fitting parameters for bandgap PL emission spectrum of nonstacked NPLs at all temperatures.

T (K)	E_{c1} (eV)	ΔE_1 (meV)	A_1	E_{c2} (eV)	ΔE_2 (meV)	A_2	Total area
290	2.406	40.9	55.1	n/a	n/a	n/a	55.1
270	2.414	40.7	58	n/a	n/a	n/a	58
240	2.422	37.2	62.4	n/a	n/a	n/a	62.4
210	2.432	33.3	66.8	n/a	n/a	n/a	66.8
180	2.444	27.9	60.8	2.418	33.6	12.3	73.1
150	2.453	24.5	62.6	2.427	25.9	15.9	78.5
125	2.461	22.4	69.2	2.433	18.8	10.2	79.4
100	2.468	20.8	71.6	2.44	17.8	13	84.6
80	2.472	20	73.7	2.444	16.5	15.9	89.6
50	2.477	18.9	76.5	2.45	17.5	24.6	101.1
20	2.480	18.5	80.9	2.453	16.6	29.5	110.4

at lower energies, is the emission from trap states, which is also typical in QDs [67]. The bandgap emission has been best fit with one or two Lorentzian curves, whereas the wide trap state emission is fit with a Gaussian at all temperatures. The fitting parameters for these features are given in Tables 4.1 and 4.2. The Lorentzian fitting function is $I = \frac{2A_1}{\pi}\frac{\Delta E_1}{4(E-E_{c1})^2+\Delta E_1^2}(+\frac{2A_2}{\pi}\frac{\Delta E_2}{4(E-E_{c2})^2+\Delta E_2^2})$ and the Gaussian fitting function is $I = \frac{A}{\Delta E\sqrt{\pi/2}} exp\left(-2\left(\frac{E-E_c}{\Delta E}\right)^2\right)$, where I is the intensity of the collected emission, E is the photon energy, E_c is the peak (center) emission photon energy, ΔE is the spectral width of the photon emission and A is the multiplying coefficient.

Tables 4.1 and 4.2 reveal that the maximum PL emission of the nonstacked NPL ensemble is at 20 K. The total area under the whole emission spectrum at this temperature is 110.4 + 226.3 = 336.7 units. We also note that multiexciton generation via absorption of a single photon is impossible because our sample is excited with a laser with photon energy of 3.30 eV (λ= 375 nm), which is less than twice the bandgap of the NPLs. Therefore, it can be realized that the QY cannot exceed unity. The spectrum at 20 K reveals that 110.4/336.7 = 32.8% of the total emission comes from the band edge, so the total QY at 20 K can be at most 32.8%. Comparing the ratios of band-edge emissions at room temperature and 20 K, we conclude that the maxium QY of nonstacked ensembles at room

Table 4.2: Gaussian fitting parameters for trap state PL emission of nonstacked NPLs at all temperatures.

T (K)	E_c (eV)	ΔE (eV)	Total area
290	1.673	0.316	40.2
270	1.668	0.32	45.6
240	1.671	0.32	47.0
210	1.678	0.341	65.8
180	1.686	0.345	82.3
150	1.692	0.356	111.4
125	1.696	0.355	151.8
100	1.7	0.357	184.9
80	1.702	0.35	198.6
50	1.705	0.352	221.4
20	1.709	0.35	226.3

temperature could be 32.8% $\times$ 55.1/110.4 = 16.3%. The calculated maximum QY is relatively lower compared to previously reported values for core CdSe NPLs [16, 17, 32, 63]. This can be explained by the reduction of PL emission under the vacuum, where there is no oxygen to passivate the NPL surfaces [37]. We-ran simulations for room temperature QY values ranging from 2% up to 16%, with interval steps of 2%.

To predict the FRET rate, we used Förster's theory for dipole-dipole energy transfer, given by Eqs. 2.1 and 2.2. As described in the previous chapter and Ref. [32], the dipole orientation factor is $\kappa^2 = 4$ and the refractive index of the medium is n = 1.8. To calculate the spectral overlap between the absorption and emission spectra of the NPLs at room temperature, the extinction coefficient of 3.1×10^{-14} cm^2 at 400 nm has been used [38]. With these parameters chosen and the QY of the nondefected NPLs varied between 0.02 and 0.16, the FRET rate has been found to be varying between $(23.8\ ps)^{-1}$ and $(3.0\ ps)^{-1}$, which is in excellent agreement with the previously reported FRET times of 6-23 ps [31]. We assumed that for a particular QY, the FRET rate does not change with the temperature. To justify this assumption, we note that the FRET rate is proportional to the exciton decay rate γ_{total}, the donor QY and the spectral overlap between the absorption and emission spectra of the NPLs. The first two of these factors increase as the temperature is lowered, whereas the spectral overlap is expected

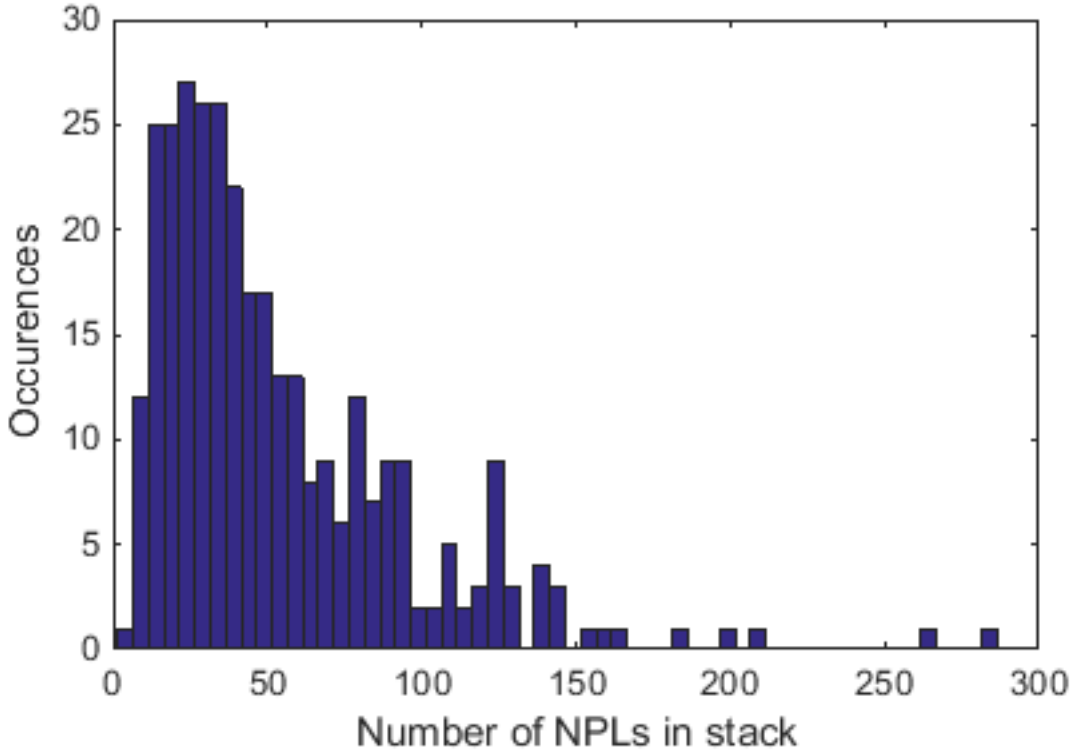

Figure 4.7: Size distribution of NPL stacks in the stacked ensemble.

to decrease considerably when it is assumed that the Stokes shift stays constant with temperature, since the emission spectrum becomes narrower with decreasing temperature.

The size distribution of the NPL stacks in terms of the number of NPLs they have are given in Figure 4.7. The size histogram has been obtained by counting the NPLs in over 300 stacks from 7 TEM images taken from the different regions of the TEM grid. The shortest stack observed has 5 NPLs, whereas the longest stack has around 280 NPLs and is longer than 1 µm in chain length.

The fraction of the defected NPLs, f, is also used as a variational parameter, similar to the QY at room temperature. As discussed previously and shown in Figure 4.5, with increasing proportion of defects, the QY and the lifetime of the NPL stacks are expected to decrease. A more systematic study of the dependence of average lifetime on the fraction of NPLs in the ensemble, f, is illustrated in Figure 4.8. For a constant trap rate $\gamma_{trap} = (35\ \text{ps})^{-1}$, increasing f causes a

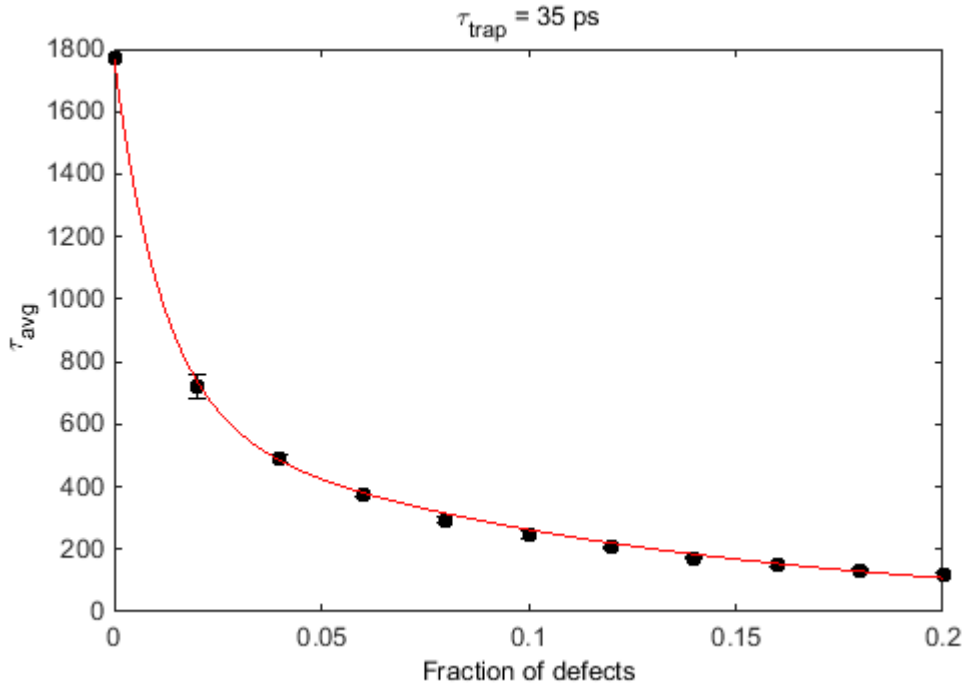

Figure 4.8: Calculated average lifetime for the stacked ensemble used in the experiment as a function of the defect fraction f, shown in black dots. The trapping rate was kept constant at (35 ps)$^{-1}$. The fit to the calculated τ_{avg} was a biexponential curve.

reduction in the PL decay time. A similar decay on the QY with increasing f is also expected.

We ran the simulations for different values of f varying between 0.1 and 0.9, with steps of 0.1. Together with 8 different QY values at the room temperature (QY_{RT}), we carried out the simulations for a total of 72 different cases. For a systematic sequence of the simulations, in each case, i.e., for each (f, QY_{RT}) pair, we ran Monte-Carlo simulations to calculate the PL lifetime and QY of the stacked NPL ensemble. In each step of the simulation, a NPL stack, whose size was randomly chosen using the size distribution given in Figure 4.7, was defined. Using the parameter f, we determined which of the NPLs in the stack were defected: Each NPL has a chance to be defected with probability f. Then, the transition probability matrix P is defined, and the PL lifetime and the QY of the NPL stack are calculated iteratively. After this was repeated for each stack, Eqs. 4.16 and 4.17 were used to calculate the overall QY and average lifetime for

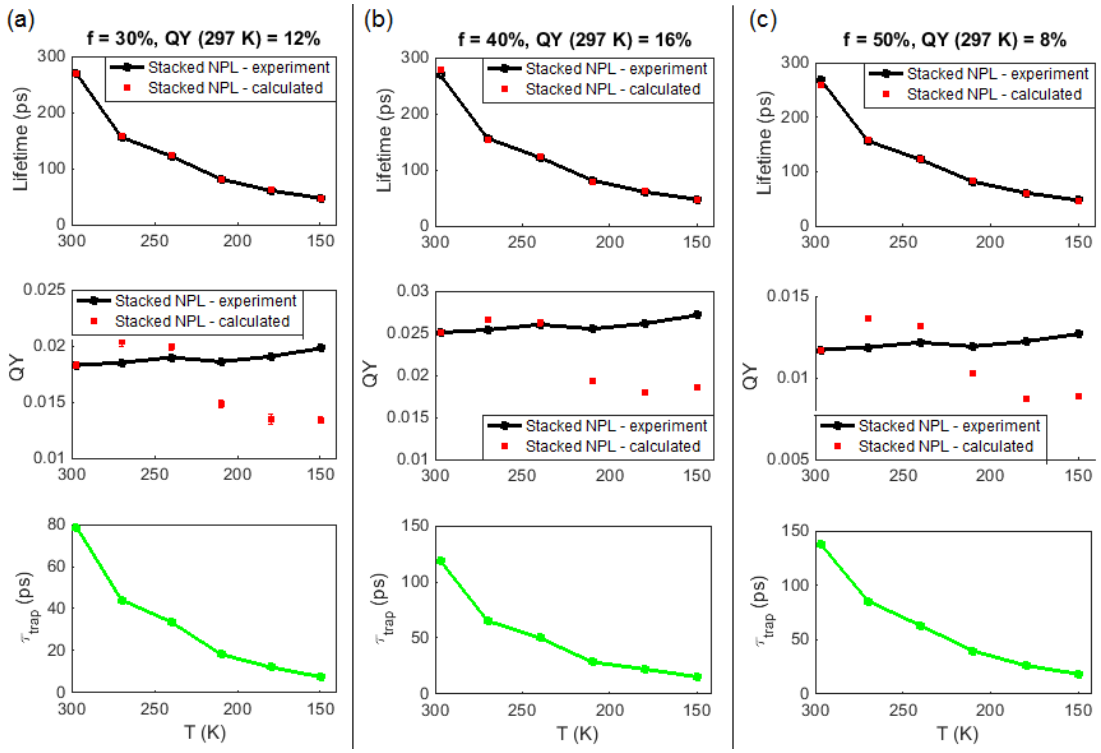

Figure 4.9: Estimated lifetimes and QYs of stacked NPL ensembles for (a) f = 0.3 and QY_{RT} = 0.12, (b) f = 0.4 and QYRT = 0.16 and (c) f = 0.5 and QY_{RT} = 0.12. The top figures show the calculated and measured lifetimes as a function of temperature. The middle figure plots the experimental QYs together with the QYs estimated using the model. The optimum τ_{trap} parameter used to match the calculated lifetimes to the experimental ones are plotted as a function of the temperature at the bottom figures.

the ensemble.

In the simulations, $\gamma_{trap} = 1/\tau_{trap}$ was used as a variational parameter. τ_{trap} changes the nonradiative recombination probability in the defected NPLs and is an important parameter that affects the average PL lifetime and QY. In our simulations, τ_{trap} was varied until the average PL lifetime at a temperature matched the experimentally found lifetime, shown in Figure 4.3(f) with red triangles. Then the corresponding ensemble QY was recorded. We repeated this procedure at all temperatures and recorded the change in QY as well as the τ_{trap} parameter that was used to match the calculation of the model with the experimental lifetime.

The simulations for a particular parameter set of f, nondefected QY, γ_{total} and γ_{trap} have been carried out on 5 ensembles, each of which consists of 200 NPL

stacks to capture the ensemble behaviour. The results of the simulations compared with the data extracted from the experiments are shown for three (f, QY_{RT}) pairs are shown in Figure 4.9. As described above, τ_{trap} at each temperature was found by sweeping it until the calculated PL lifetime was a match to the measured PL lifetime. The corresponding QY of the stacked ensemble was then calculated with this τ_{trap} value. When calculating the QY as a function of the temperature, the calculated room-temperature QY of the stacked NPL ensemble was used as a trivial solution, i.e., the experimental QY of the stacked ensemble at RT was assumed to be equal to the calculated room-temperature QY, and QYs at other temperatures were calculated by multiplying the room-temperature QY by the relative bandgap emission change factors, shown in Figure 4.3(c) with red triangles.

It can be observed in Figure 4.9 that, with the use of the optimum τ_{trap} value at each temperature, the estimated QYs exhibit reasonably good agreement with the experimental data. There is an excellent agreement between the calculated and measured values for 270 and 240 K, whereas the calculated QYs are off by about 30% for the lower temperatures. This is the general behaviour observed for all (f, QY) pairs tested. The calculated QY of the stacked ensemble agrees well with the experimental values at 270 and 240 K, starts to diverge at 210 K and is about 30% lower than the measured data at 180 and 150 K. There are several reasons for the difference between the experimental results and calculations. First, with decays getting faster at lower temperatures, the exponential fittings for the decays become less reliable since the FWHM of the excitation laser, which is about 220 ps, becomes comparable to that of the PL decay, which makes reconvolution fitting difficult and more prone to error. The second reason is the error introduced by using the amplitude-averaged PL lifetime when carrying out the calculations and analyses, instead of taking different exponential components into account. A more complete analysis could be possible by considering energy transfer dynamics with fluorophores in the ensemble having different transient decay kinetics. However, the complex decay kinetics of NPLs have not yet been fully understood. Therefore, here we carried out the analysis by using average lifetimes. Nevertheless, when characterizing the energy transfer,

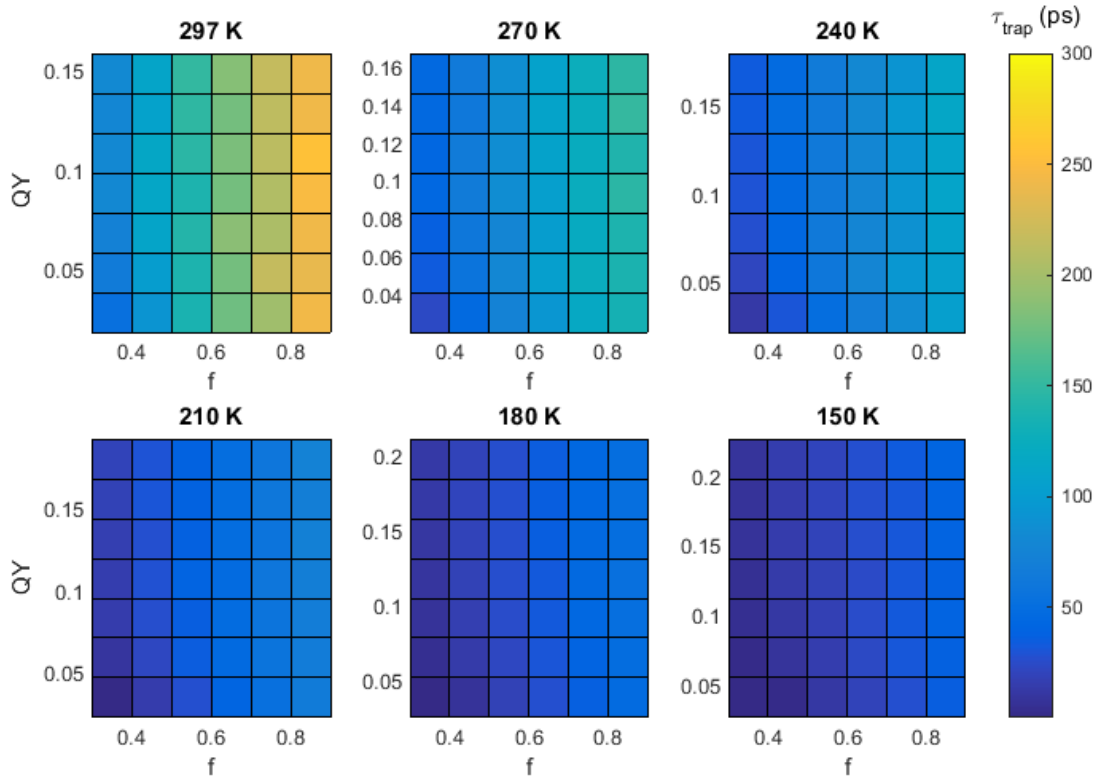

Figure 4.10: Computed optimum trapping times calculated at each temperature, for different defect fraction - QY pairs.

the use of amplitude-average lifetime is a legitimate approach in the presence of multiexponential decays [51].

Figure 4.10 displays τ_{trap} parameters that match the calculated and measured PL lifetimes of stacked NPLs for all the studied temperatures. When f $\leq$ 0.2, the calculated decay times could not be matched to the experimental values, no matter how small the tested τ_{trap} was chosen. Even when τ_{trap} was on the order of femtoseconds, the calculated lifetimes were still considerably larger than the measured lifetimes. Hence, the results could not be calculated properly for f = 0.1 and f = 0.2, and were not plotted in the figure. For the parameter range in which the lifetime and QY was estimated properly, the optimum τ_{trap} took values between 70 fs and 300 ps. These upper and lower bounds are out of range for the typical hole trapping times, which is expected to be on the order of 10 ps [63]. This can be used to estimate the actual QY and the fraction of the defected NPLs.

As seen in Figure 4.10 the calculated τ_{trap} smoothly changes with f and QY. We observe that τ_{trap} increases with increasing percentage of the defected NPLs. This is the expected behaviour of τ_{trap} as discussed previously. With more trap sites in the NPL stack, smaller trapping rates suffice to suppress the increase in photoluminescence intensity. However, when the defects are sparse, the probability that an exciton visits a trap sites decreases; so, for the suppression of PL increase, an increased probability of nonradiative recombination in the defected NPLs is needed. Similarly, with increasing QY, τ_{trap} decreases because FRET rate is proportional to QY, and faster FRET enables more frequent arrivals to trap sites, resulting in more of the excitons to decay nonradiatively. However, according to our model, the energy is transferred at the same rate in the defected NPLs as the non-defected ones; therefore, increasing γ_{FRET} continuously might not imply that the PL intensity will keep being suppressed. In fact, it was observed when testing the model that if γ_{FRET} is increased continuously so that it becomes much larger than γ_{trap}, the suppression of PL intensity is observed to a limited extent. The reason for this behaviour is that, when $\gamma_{FRET} \gg \gamma_{trap}$, virtually all of the excitons visiting the trap sites are retransferred to another NPL before they are "caught" in a trap, rendering the trap sites ineffective.

The final important observation is that the trapping rate increases with decreasing temperature. This can be explained by the reduction of thermal energy of carriers at lower temperatures. With smaller thermal energy, the excitons become more likely to get trapped when there is a surface trap [45]. Over 5-fold increase in the trap state emission when the temperature is reduced from 297 to 20 K (see Figure 4.6) also supports the increased trapping rate at lower temperatures. Another possible reason is that some of the NPLs, which are non-defected at first, start to act as defected when the temperature is reduced because of the trap sites that might be activated only at low temperatures. In this case, the fraction of the defected NPLs would also be a function of the temperature.

4.3 Conclusion

To sum up, the steady-state PL and the time-resolved emission kinetics in the stacked NPLs as well as in the nonstacked ones have been systematically investigated at various temperatures ranging from 150 to 297 K. We compared the experimental measurements for the nonstacked and stacked NPL ensembles. We observed that the PL decay is much faster in the stacked NPLs than in the nonstacked NPLs at all temperatures. Furthermore, the PL intensity enhancement factor when the temperature is reduced from 297 to 150 K was only 1.08 in the stacked NPL ensemble, whereas there was a 1.4-fold increase in the PL intensity of the nonstacked NPL ensemble. In order to explain the difference between the PL decay times and temperature-dependent PL intensity changes of the nonstacked and stacked NPLs, we developed a theoretical model that considers the excitonic transitions in a NPL stack as a Markovian process. In this model, we took fast FRET between the neighbouring NPLs in a stack together with charge trapping that is known to take place in some of the NPLs into account. Using this model, we were able to estimate the QY and average PL lifetime of a stacked NPL ensemble as well as the rate of charge trapping as a function of the temperature. The agreement between the model's predictions and the experimental data is reasonably good. The model shows that the suppression of the increase in the PL intensity is possible when the trapping rate increases with decreasing temperature. Our Markov chain-based model presents a new way for transient and steady-state characterization of the exciton kinetics in these NPL stacks.

Chapter 5

Conclusion

In this thesis, we studied the changes in the excitonic dynamics of colloidal NPLs when they are stacked. Even with partial stacking in the NPL ensemble, there is significant quenching in the photoluminescence intensity and reduction in the photoluminescence lifetime. We also demonstrated that temperature-dependent PL intensity trend of completely stacked NPLs differs greatly from that of non-stacked ones. Our models successfully explain these changes using fast exciton transport in a stack accompanied by occasional charge trapping. Here, FRET-assisted exciton trapping was shown to have a significant effect on the transient and steady-state exciton dynamics of NPL stacks.

Due to their one-dimensional quantum confinement and magic sized thickness, it is possible to obtain very narrow PL spectra from NPLs. Since there is almost no inhomogeneous broadening in the emission linewidth caused by size variations, energy transfer within NPLs of the same thickness causes no or little red shift in PL spectrum. This means that, while an exciton is being transferred, it does not continuously lose energy as in FRET within QD clusters with QDs of varying sizes, but keeps its energy during the transport. However, our models show that existence of a few trap sites in the stacks becomes capable of trapping many excitons due to the high rate of FRET in the NPL stacks. Using either of the models proposed, we can estimate the fraction of NPLs having a trapping site.

This can be used in the characterization of the NPL ensemble.

High-rate FRET between neighbouring NPLs in a stack may enable fast exciton transportation through micrometer-long superlattices. Such a mechanism could be very useful for light harvesting and generation applications. However, as discussed above, when there are traps on the way, a significant number of excitons are likely to be lost to heat through nonradiative processes, resulting in reduced efficiencies. Therefore, when using the NPLs in stacked morphologies, one should make sure that the fraction of the defected NPLs in the ensemble is tolerable so that not many excitons are wasted during the transportation process. High-quality NPLs that have a low subpopulation of defects are then ideal for creating giant superlattices for exciton transport. The future work will focus on making ordered superlattices (chains) of NPLs, generating a hierarchical superstructure of NPLs, and understanding their excitonic dynamics.

Bibliography

[1] D. V. Talapin, J.-S. Lee, M. V. Kovalenko, and E. V. Shevchenko, "Prospects of colloidal nanocrystals for electronic and optoelectronic applications," *Chemical reviews*, vol. 110, no. 1, pp. 389–458, 2009.

[2] M. V. Kovalenko, L. Manna, A. Cabot, Z. Hens, D. V. Talapin, C. R. Kagan, V. I. Klimov, A. L. Rogach, P. Reiss, D. J. Milliron, P. Guyot-Sionnnest, G. Konstantatos, W. J. Parak, T. Hyeon, B. A. Korgel, C. B. Murray, and W. Heiss, "Prospects of Nanoscience with Nanocrystals," *ACS Nano*, vol. 9, pp. 1012–1057, feb 2015.

[3] A. L. Efros and A. L. Efros, "Interband absorption of light in a semiconductor sphere," *Soviet Physics Semiconductors-Ussr*, vol. 16, no. 7, pp. 772–775, 1982.

[4] L. Brus, "Electronic wave functions in semiconductor clusters: experiment and theory," *The Journal of Physical Chemistry*, vol. 90, pp. 2555–2560, jun 1986.

[5] C. B. Murray, D. J. Norris, and M. G. Bawendi, "Synthesis and characterization of nearly monodisperse CdE (E = sulfur, selenium, tellurium) semiconductor nanocrystallites," *Journal of the American Chemical Society*, vol. 115, pp. 8706–8715, sep 1993.

[6] A. P. Alivisatos, "Perspectives on the Physical Chemistry of Semiconductor Nanocrystals," *The Journal of Physical Chemistry*, vol. 3654, no. 95, pp. 13226–13239, 1996.

[7] D. V. Talapin, J. H. Nelson, E. V. Shevchenko, S. Aloni, B. Sadtler, and A. P. Alivisatos, "Seeded Growth of Highly Luminescent CdSe / CdS Nanoheterostructures with Rod and Tetrapod Morphologies," *Nano Letters*, vol. 7, no. 10, pp. 2951–2959, 2007.

[8] V. L. Colvin, M. C. Schlamp, and A. P. Alivisatos, "Light-emitting diodes made from cadmium selenide nanocrystals and a semiconducting polymer," *Nature*, vol. 370, no. 6488, pp. 354–357, 1994.

[9] X. Dai, Z. Zhang, Y. Jin, Y. Niu, H. Cao, X. Liang, L. Chen, J. Wang, and X. Peng, "Solution-processed, high-performance light-emitting diodes based on quantum dots," *Nature*, vol. 515, pp. 96–99, nov 2014.

[10] A. J. Nozik, "Quantum dot solar cells," *Physica E: Low-dimensional Systems and Nanostructures*, vol. 14, no. 1, pp. 115–120, 2002.

[11] D. V. Talapin and C. B. Murray, "PbSe Nanocrystal Solids for n- and p-Channel Thin Film Field-Effect Transistors," *Science*, vol. 310, pp. 86–89, oct 2005.

[12] V. I. Klimov, "Optical Gain and Stimulated Emission in Nanocrystal Quantum Dots," *Science*, vol. 290, pp. 314–317, oct 2000.

[13] U. Resch-Genger, M. Grabolle, S. Cavaliere-Jaricot, R. Nitschke, and T. Nann, "Quantum dots versus organic dyes as fluorescent labels," *Nature Methods*, vol. 5, pp. 763–775, sep 2008.

[14] C. A. Leatherdale, W.-K. Woo, F. V. Mikulec, and M. G. Bawendi, "On the Absorption Cross Section of CdSe Nanocrystal Quantum Dots," *The Journal of Physical Chemistry B*, vol. 106, pp. 7619–7622, aug 2002.

[15] S. Ithurria and B. Dubertret, "Quasi 2D Colloidal CdSe Platelets with Thicknesses Controlled at the Atomic Level," *Journal of the American Chemical Society*, vol. 130, pp. 16504–16505, 2008.

[16] S. Ithurria, M. D. Tessier, B. Mahler, R. P. S. M. Lobo, B. Dubertret, and A. L. Efros, "Colloidal nanoplatelets with two-dimensional electronic structure," *Nature Materials*, vol. 10, no. 10, pp. 936–941, 2011.

[17] M. D. Tessier, C. Javaux, I. Maksimovic, V. Loriette, and B. Dubertret, "Spectroscopy of single CdSe nanoplatelets," *ACS Nano*, vol. 6, no. 8, p. 67516758, 2012.

[18] P. P. Pompa, L. Martiradonna, A. Della Torre, F. Della Sala, L. Manna, M. De Vittorio, F. Calabi, R. Cingolani, and R. Rinaldi, "Metal-enhanced fluorescence of colloidal nanocrystals with nanoscale control," *Nature Nano*, vol. 1, pp. 126–130, nov 2006.

[19] D. V. Guzatov, S. V. Vaschenko, V. V. Stankevich, A. Y. Lunevich, Y. F. Glukhov, and S. V. Gaponenko, "Plasmonic enhancement of molecular fluorescence near silver nanoparticles: theory, modeling, and experiment," *The Journal of Physical Chemistry C*, vol. 116, no. 19, pp. 10723–10733, 2012.

[20] T. Ozel, S. Nizamoglu, M. A. Sefunc, O. Samarskaya, I. O. Ozel, E. Mutlugun, V. Lesnyak, N. Gaponik, A. Eychmuller, S. V. Gaponenko, and H. V. Demir, "Anisotropic emission from multilayered plasmon resonator nanocomposites of isotropic semiconductor quantum dots," *ACS nano*, vol. 5, pp. 1328–34, feb 2011.

[21] R. M. Clegg, "Fluorescence resonance energy transfer," *Current Opinion in Biotechnology*, vol. 6, no. 1, pp. 103–110, 1995.

[22] C. R. Kagan, C. B. Murray, M. Nirmal, and M. G. Bawendi, "Electronic Energy Transfer in CdSe Quantum Dot Solids," *Physical Review Letters*, vol. 76, no. 9, pp. 1517–1520, 1996.

[23] W. C. W. Chan and S. Nie, "Quantum Dot Bioconjugates for Ultrasensitive Nonisotopic Detection," *Science*, vol. 281, pp. 2016–2018, sep 1998.

[24] M. Bruchez, M. Moronne, P. Gin, S. Weiss, and A. P. Alivisatos, "Semiconductor Nanocrystals as Fluorescent Biological Labels," *Science*, vol. 281, pp. 2013–2016, sep 1998.

[25] A. R. Clapp, I. L. Medintz, J. M. Mauro, B. R. Fisher, M. G. Bawendi, and H. Mattoussi, "Fluorescence Resonance Energy Transfer Between Quantum Dot Donors and Dye-Labeled Protein Acceptors," *Journal of the American Chemical Society*, vol. 126, pp. 301–310, January 2004.

[26] D. Zhou, J. D. Piper, C. Abell, D. Klenerman, D.-J. Kang, and L. Ying, "Fluorescence resonance energy transfer between a quantum dot donor and a dye acceptor attached to DNA," *Chemical Communications*, no. 38, pp. 4807–4809, 2005.

[27] S. A. Crooker, J. A. Hollingsworth, S. Tretiak, and V. I. Klimov, "Spectrally resolved dynamics of energy transfer in quantum-dot assemblies: Towards engineered energy flows in artificial materials," *Physical Review Letters*, vol. 89, no. 18, 2002.

[28] N. Reitinger, A. Hohenau, S. Köstler, J. R. Krenn, and A. Leitner, "Radiationless energy transfer in CdSe/ZnS quantum dot aggregates embedded in PMMA," *Physica Status Solidi (a)*, vol. 208, pp. 710–714, mar 2011.

[29] B. Abecassis, M. D. Tessier, P. Davidson, and B. Dubertret, "Self-Assembly of CdSe Nanoplatelets into Giand Micrometer-Scale Needles Emitting Polarized Light," *Nano Letters*, vol. 14, pp. 710–715, 2013.

[30] M. D. Tessier, L. Biadala, C. Bouet, S. Ithurria, B. Abecassis, and B. Dubertret, "Phonon Line Emission Revealed by Self-Assembly of Colloidal Nanoplatelets," *ACS Nano*, vol. 7, no. 4, pp. 3332–3340, 2013.

[31] C. E. Rowland, I. Fedin, H. Zhang, S. K. Gray, A. O. Govorov, D. V. Talapin, and R. D. Schaller, "Picosecond energy transfer and multiexciton transfer outpaces Auger recombination in binary CdSe nanoplatelet solids," *Nature Materials*, vol. 14, pp. 484–489, 2015.

[32] B. Guzelturk, O. Erdem, M. Olutas, Y. Kelestemur, and H. V. Demir, "Stacking in Colloidal Nanoplatelets: Tuning Excitonic Properties," *ACS Nano*, vol. 8, no. 12, pp. 12524–12533, 2014.

[33] L. T. Kunneman, J. M. Schins, S. Pedetti, H. Heuclin, F. C. Grozema, A. J. Houtepen, B. Dubertret, and L. D. A. Siebbeles, "Nature and Decay Pathways of Photoexcited States in CdSe and CdSe/CdS Nanoplatelets," *Nano Letters*, vol. 14, no. 12, pp. 7039–7045, 2014. PMID: 25366327.

[34] M. Olutas, B. Guzelturk, Y. Kelestemur, A. Yeltik, S. Delikanli, and H. V. Demir, "Lateral Size-Dependent Spontaneous and Stimulated Emission Properties in Colloidal CdSe Nanoplatelets," *ACS Nano*, vol. 9, no. 5, pp. 5041–5050, 2015.

[35] A. W. Achtstein, A. V. Prudnikau, M. V. Ermolenko, L. I. Gurinovich, S. V. Gaponenko, U. Woggon, A. V. Baranov, M. Y. Leonov, and I. D. Rukhlenko, "Nanocrystals: A Comparative Study of CdSe Colloidal Quantum Dots, Nanorods, and Nanoplatelets," *ACS Nano*, vol. 8, no. 8, pp. 7678–7686, 2014.

[36] S. Ithurria, G. Bousquet, and B. Dubertret, "Continuous Transition from 3D to 1D Confinement Observed during the Formation of CdSe Nanoplatelets," *Journal of the American Chemical Society*, vol. 133, pp. 3070–3077, 2011.

[37] M. Lorenzon, S. Christohoulou, G. Vaccaro, J. Pedrini, F. Meinardi, I. Moreels, and S. Brovelli, "Reversed oxygen sensing using colloidal quantum wells towards highly emissive photoresponsive varnishes," *Nature Communications*, vol. 6, 2015.

[38] C. She, I. Fedin, D. S. Dolzhnikov, A. Demortie, R. D. Schaller, M. Pelton, and D. V. Talapin, "Low-Threshold Stimulated Emission Using Colloidal Quantum Wells," *Nano Letters*, vol. 14, pp. 2772–2777, 2014.

[39] C. Bouet, B. Mahler, B. Nadal, B. Abecassis, M. D. Tessier, S. Ithurria, X. Xu, and B. Dubertret, "Two-Dimensional Growth of CdSe Nanocrystals, from Nanoplatelets to Nanosheets," *Chemistry of Materials*, vol. 25, pp. 639–645, 2013.

[40] B. Zhou, G. Xiao, X. Yang, Q. Li, K. Wang, and Y. Wang, "Pressure-dependent optical behaviors of colloidal CdSe nanoplatelets," *Nanoscale*, vol. 7, no. 19, pp. 8835–8842, 2015.

[41] L. T. Kunneman, M. D. Tessier, H. Heuclin, B. Dubertret, Y. V. Aulin, F. C. Grozema, J. M. Schins, and L. D. A. Siebbeles, "Bimolecular Auger Recombination of Electron - Hole Pairs in Two-Dimensional CdSe and

CdSe/CdZnS Core/Shell Nanoplatelets," *The Journal of Physical Chemistry Letters*, vol. 4, pp. 3574–3578, 2013.

[42] Z. Chen, B. Nadal, B. Mahler, H. Aubin, and B. Dubertret, "Quasi-2D Colloidal Semiconductor Nanoplatelets for Narrow Electroluminescence," *Advanced Functional Materials*, vol. 8, no. 7, pp. 295–302, 2014.

[43] B. Guzelturk, Y. Kelestemur, M. Olutas, S. Delikanli, and H. V. Demir, "Amplified Spontaneous Emission and Lasing in Colloidal Nanoplatelets," *ACS Nano*, vol. 8, no. 7, pp. 6599–6605, 2014.

[44] B. Mahler, B. Nadal, C. Bouet, G. Patriarche, and B. Dubertret, "Core/Shell Colloidal Semiconductor Nanoplatelets," *Journal of the American Chemical Society*, vol. 134, pp. 18591–18598, 2012.

[45] M. D. Tessier, B. Mahler, B. Nadal, H. Heuclin, S. Pedetti, and B. Dubertret, "Spectroscopy of Colloidal Semiconductor Core/Shell Nanoplatelets with High Quantum Yield," *Nano Letters*, vol. 13, p. 33213328, 2013.

[46] A. Prudnikau, A. Chuvilin, and M. Artemyev, "CdSe-CdS Nanoheteroplatelets with Effiecient Photoexcitation of Central CdSe Region Through Epitaxially Grown CdS Wings," *Journal of the American Chemistry Society*, vol. 135, pp. 14476–14479, 2013.

[47] M. D. Tessier, P. Spinicelli, D. Dupont, G. Patriarche, S. Ithurria, and B. Dubertret, "Efficient Exciton Concentrators Built from Colloidal Core/Crown CdSe/CdS Semiconductor Nanoplatelets," *Nano Letters*, vol. 13, pp. 207–213, 2014.

[48] Y. Kelestemur, M. Olutas, S. Delikanli, B. Guzelturk, M. Z. Akgul, and H. V. Demir, "Type-II Colloidal Quantum Wells: CdSe/CdTe Core/Crown Heteronanoplatelets," *Journal of Physical Chemistry C*, vol. 119, no. 4, pp. 2177–2185, 2015.

[49] S. Delikanli, B. Guzelturk, P. L. Hernandez-Martinez, T. Erdem, Y. Kelestemur, M. Olutas, M. Z. Akgul, and H. V. Demir, "Continuously Tunable Emission in Inverted Type-I CdS/CdSe Core/Crown Semiconductor Nanoplatelets," *Advanced Functional Materials*, 2015.

[50] T. Förster, "Zwischenmolekulare Energiewanderung und Fluoreszenz," *Annalen der Physik*, vol. 437, pp. 55–75, 1948.

[51] J. R. Lakowicz, *Principles of Fluorescence Spectroscopy*. Springer, 3 ed., 2006.

[52] B. Guzelturk, M. Olutas, S. Delikanli, Y. Kelestemur, O. Erdem, and H. V. Demir, "Nonradiative energy transfer in colloidal CdSe nanoplatelet films," *Nanoscale*, vol. 7, no. 6, pp. 2545–2551, 2015.

[53] V. V. Didenko, "DNA Probes Using Fluorescence Resonance Energy Transfer (FRET): Designs and Applications," *BioTechniques*, vol. 31, no. 5, pp. 1106–1121, 2001.

[54] R. B. Sekar and A. Periasamy, "Fluorescence resonance energy transfer (FRET) microscopy imaging of live cell protein localizations," *The Journal of cell biology*, vol. 160, pp. 629–633, March 2003.

[55] T. Franzl, T. A. Klar, S. Schietinger, A. L. Rogach, and J. Feldmann, "Exciton Recycling in Graded Gap Nanocrystal Structures," *Nano Letters*, vol. 4, no. 9, pp. 1599–1603, 2004.

[56] A. Yekta, J. Duhamel, and M. A. Winnik, "Dipole-dipole electronic energy transfer. Fluorescence decay functions for arbitrary distributions of donors and acceptors: systems with planar geometry," *Chemical Physics Letters*, vol. 235, pp. 119–125, 1995.

[57] O. J. Rolinski and D. J. S. Birch, "Determination of acceptor distribution from fluorescence resonance energy transfer: Theory and simulation," *The Journal of Chemical Physics*, vol. 112, no. 20, 2000.

[58] Y. Shirasaki, G. J. Supran, M. G. Bawendi, and V. Bulovic, "Emergence of colloidal quantum-dot light-emitting technologies," *Nature Photonics*, vol. 7, no. 1, 2013.

[59] P. O. Anikeeva, C. F. Madigan, J. E. Halpert, M. Bawendi, and V. Bulovic, "Electronic and excitonic processes in light-emitting devices based on organic

materials and colloidal quantum dots," *Physical Review B*, vol. 78, no. 8, 2008.

[60] D. R. Lutz, K. A. Nelson, C. R. Gochanour, and M. D. Fayer, "Electronic excited state energy transfer, trapping by dimers and fluorescence quenching in concentrated dye solutions: Picosecond transient grating experiments," *Chemical Physics*, vol. 58, pp. 325–334, 1981.

[61] R. F. Loring, H. C. Andersen, and M. D. Fayer, "Electronic excited state transport and trapping in solution," *The Journal of Chemical Physics*, vol. 76, no. 4, pp. 2915–2027, 1982.

[62] A. Sanchez, F. Dominguez-Adame, and E. Macia, "Excitation decay in 1D disordered systems," *Physical Review B*, vol. 51, no. 1, pp. 173–178, 1995.

[63] A. W. Achtstein, A. Schliwa, A. Prudnikau, M. Hardzei, M. V. Artemyev, C. Thomsen, and U. Woggon, "Electronic structure and exciton-phonon interaction in two-dimensional colloidal CdSe nanosheets.," *Nano Letters*, vol. 12, pp. 3151–3157, jun 2012.

[64] L. Kulak and C. Bojarski, "Forward and reverse electronic energy transport and trapping in solution. I. Theory," *Chemical Physics*, vol. 191, no. 13, pp. 43–66, 1995.

[65] L. Kulak and C. Bojarski, "Forward and reverse electronic energy transport and trapping in solution. II. Numerical results and Monte Carlo simulations," *Chemical Physics*, vol. 191, no. 13, pp. 67–86, 1995.

[66] E. W. Montroll, "Random Walks on Lattices. III. Calculation of First-Passage Times with Application to Exciton Trapping on Photosynthetic Units," *Journal of Mathematical Physics*, vol. 10, no. 4, pp. 753–765, 1969.

[67] P. Kambhampati, "Hot Exciton Relaxation Dynamics in Semiconductor Quantum Dots: Radiationless Transitions on the Nanoscale," *The Journal of Physical Chemistry C*, vol. 115, pp. 22089–22109, nov 2011.